frontiers | Frontiers in Chemical Engineering

TYPE Review
PUBLISHED 08 August 2024
DOI 10.3389/fceng.2024.1430773

OPEN ACCESS

EDITED BY
Patricia Luis,
Université Catholique de Louvain, Belgium

REVIEWED BY
Diana Sannino,
University of Salerno, Italy
Zhengwei Zhou,
Changzhou University, China
Saravanakumar Karunamoorthy,
Kyungpook National University, Republic of Korea

*CORRESPONDENCE
Inmaculada Ortiz,
ortizi@unican.es

RECEIVED 10 May 2024
ACCEPTED 22 July 2024
PUBLISHED 08 August 2024

CITATION
González-Fernández C, Bringas E, Rivero MJ and Ortiz I (2024), Revealing the role of magnetic materials in light-driven advanced oxidation processes: enhanced degradation of contaminants and facilitated magnetic recovery.
Front. Chem. Eng. 6:1430773.
doi: 10.3389/fceng.2024.1430773

Revealing the role of magnetic materials in light-driven advanced oxidation processes: enhanced degradation of contaminants and facilitated magnetic recovery

Cristina González-Fernández, Eugenio Bringas, María J. Rivero and Inmaculada Ortiz*

Departamento de Ingenierías Química y Biomolecular, Universidad de Cantabria, Santander, Spain

Semiconductor photocatalysis, heterogeneous photo-Fenton and heterogeneous photocatalytic persulfate activation are light-driven advanced oxidation processes (AOPs) that have attracted much attention as promising technologies in wastewater treatment. Nevertheless, their large-scale application still faces several challenges, including the need to separate the catalyst from the treated water. In this regard, composite catalysts made up of semiconductor and magnetic materials have been understood as a potential alternative since the resulting magnetic photocatalysts can be easily separated from the medium by applying an external magnetic field. Interestingly, apart from facilitating the photocatalyst retrieval, the magnetic components could also be involved in the photocatalytic process. However, while the magnetic separation ability has been widely highlighted, other functions of the magnetic constituents remain obscure. This work, which covers the last 6 years of research, provides a comprehensive review on the magnetically assisted photocatalytic degradation of organic pollutants from water. Specifically, the magnetic photocatalysts that are commonly employed for that purpose are presented and the different roles of their magnetic constituents (roughly grouped as retrieval assistance, active catalyst, conduction medium or activator) are discussed. Furthermore, the importance of designing magnetic separators for attaining the photocatalyst retrieval is also emphasized. Collectively, this study could supply an avenue for developing magnetic photocatalysts that take advantage of both roles of magnetic materials, which can contribute to accomplish a more efficient pollutant degradation.

KEYWORDS

magnetic photocatalyst, magnetic separation, photocatalysis, wastewater, organic pollutants

1 Introduction

Global development and a better lifestyle come at the price of water pollution, which has emerged as a serious environmental issue. Particularly, the industrialization, rapid population growth and several anthropogenic activities (e.g., agriculture) have led to the discharge of pollutants in aquatic ecosystems, thus degrading the quality of water resources (Ahmadpour et al., 2020; Arman et al., 2021; Khosravani Goshtasb et al., 2022; Surana et al.,

2022; Vale et al., 2022). A group of great interest is constituted by the so-called Contaminants of Emerging Concern (CECs), which comprise an extensive variety of micropollutants (including pharmaceuticals, personal care products, biocides, pesticides, herbicides, etc.); they have been detected in surface, ground and drinking water (Chávez et al., 2020; Tsaridou and Karabelas, 2021; Adeola et al., 2022). The adverse impacts that CECs pose on the environment and human health cause that their presence in water bodies raises concern worldwide. Hence, there is an urgent need to develop strategies to remove these pollutants from water (Cheng et al., 2021; Adeola et al., 2022; Morin-Crini et al., 2022).

Light-driven advanced oxidation processes (AOPs) have gained great recognition for that purpose; they constitute a family of technologies that are based on the production of highly reactive oxygen species, including hydroxyl radicals ($^{\bullet}OH$) and sulfate radicals ($SO_4^{\bullet-}$) to convert pollutants into small compounds that are more easily degradable or biodegradable (Thomas et al., 2021; Guo et al., 2022). Light-driven AOPs comprise several technologies, such as photocatalysis, Fenton and Fenton-like processes or persulfates activation, which have proved their potential for degrading organic pollutants (Qi et al., 2016; Dewil et al., 2017; Ahmadpour et al., 2020; Guo et al., 2022). Briefly, semiconductor photocatalysis relies on the generation of electron-hole (e^-/h^+) pairs when the material is exposed to light with energy equal to or greater than their band gap (Eg). These photogenerated e^-/h^+ pairs can migrate to the catalyst's surface to form oxidizing species ($^{\bullet}OH$ and superoxide radicals, $O_2^{\bullet-}$) that play a primary role in the degradation of organic matter (Sonu et al., 2019; Younis and Kim, 2020). Hence, the selection of photocatalysts will focus on materials with advantageous properties, such as: (i) visible-light activity, (ii) photostability, (iii) non-toxicity, (iv) low recombination rate of e^-/h^+ pairs, (v) biological and chemical inactivity, and (vi) easy recovery from the purified water (Bhatkhande et al., 2002; Behnajady et al., 2012; Bahmani et al., 2020; Bielan et al., 2021). In other words, the dream photocatalyst should demonstrate both a high photocatalytic ability under visible light irradiation and its easy retrievability after use (Mahato et al., 2019; Kamali et al., 2022; Feng et al., 2023). On the other hand, the heterogeneous Fenton process involves the production of $^{\bullet}OH$ radicals through the decomposition of hydrogen peroxide via redox reactions involving iron ions (Fe^{2+}/Fe^{3+}) at the interface of iron-based catalysts (Thomas et al., 2021; Radji et al., 2022). The yield of the Fenton process can be improved applying light, which leads to photo-Fenton process (Jiang Y. et al., 2022; Machado et al., 2023; Wu et al., 2023). Specifically, the inclusion of light irradiation boosts the performance of the Fenton process by increasing the production of $^{\bullet}OH$ radicals through H_2O_2 photolysis and accelerating the regeneration of Fe^{2+} ions (O'Dowd and Pillai, 2020; Ganiyu et al., 2022; Wu et al., 2023; Bule Možar et al., 2024). In contrast to photocatalysis and photo-Fenton, persulfate-based AOPs operate on the principle of activating persulfates (e.g., peroxymonosulfate, PMS, or peroxydisulfate, PDS) to produce $SO_4^{\bullet-}$ radicals. Different strategies can be pursued for persulfate activation, including, ultraviolet radiation, e^-/h^+ pairs from the photocatalyst, or transition metals based catalysts (Kohantorabi et al., 2021; Guo et al., 2022; Klu et al., 2022; Moradi et al., 2022; Oyekunle et al., 2022).

In light of the concise overview of several AOPs previously mentioned, it is evident that most of the research on the catalytic degradation of pollutants has been carried out working with solid semiconductors suspended in the aqueous medium; therefore, after treatment, the catalysts must be efficiently separated from the liquid (He et al., 2019; Bielan et al., 2021). Nevertheless, the retrieval and recycling of the photocatalyst after the degradation process, which are of paramount importance for making the process cost-effective, represent an ongoing challenge that needs to be further explored (Iglesias et al., 2016; Abdel-Wahed et al., 2020; Bielan et al., 2021). Filtration and centrifugation have been used for the retrieval of the photocatalyst. However, the high cost and energy consumption of these additional operations call for the development of more efficient strategies (Wu et al., 2019; Lendzion-Bielun et al., 2020). If the photocatalytic material contains constituents of magnetic character, implementation of magnetic field-based separation provides a convenient avenue for accomplishing its successful retrieval (Bielan et al., 2021). Hence, compositing semiconductors with magnetic materials enables the successful retrieval of the resulting magnetic photocatalyst by applying external magnetic fields. Besides the advantageous separation and recovery of the magnetic photocatalyst, it has been reported that the magnetic component could participate in the photocatalytic degradation of pollutants, thus enhancing the photocatalyst's performance (Lendzion-Bielun et al., 2020; Moradi et al., 2022). Given that the magnetic constituent could fulfill several roles (roughly grouped as retrieval assistance and photocatalytic), recognizing these functions is of utmost importance for designing and synthesizing more efficient photocatalysts. In a previous work of our research group (Gómez-Pastora et al., 2017a), the use of magnetic photocatalysts for water treatment was outlined and their promising possibilities for that application were highlighted. However, such study was mainly focused on the photocatalytic properties of these composites and their synthesis methods, thus the photocatalytic function of the magnetic materials was not investigated and the magnetic recovery of the photocatalyst was slightly addressed.

Motivated by this lack of knowledge, the present work aims at providing a comprehensive overview about the magnetically assisted photocatalytic degradation of organic pollutants from water. We specially focus on two key features of photocatalysis involving magnetic photocatalysts, namely, unveiling the possible roles of photocatalyst's magnetic constituents (coarsely categorized as retrieval assistance and photocatalytic), and progressing in the efficient recovery of the photocatalyst after use. Firstly, photocatalysts whose magnetic component exclusively contributes to facilitate their retrieval are introduced. The following section provides insights into the photocatalytic functions that the magnetic materials could accomplish. Additionally, an overall picture of the magnetic recovery of the photocatalysts is given, with a special attention to the promising magnetic separators that could be used for that purpose. Finally, we close this work highlighting several key challenges and prospects of the performance and separation of magnetic photocatalysts. Overall, the present study could pave the way for the rational design of magnetic photocatalysts that apart from being easily collected after use demonstrate enhanced photocatalytic ability by benefiting from the photocatalytic roles of the magnetic materials.

TABLE 1 Studies focused on the retrieval assistance role of the magnetic constituents of photocatalysts.

Photocatalyst	Magnetic composite morphology	Ms (emu/g)	Eg (eV)	Substrate	Light source	Performance[a] (%)	Ref.
2D/2D TiO_2-GO-$ZnFe_2O_4$	GO layers combined with 2D TiO_2 and embedded with $ZnFe_2O_4$	n.s	~2.85	Ibuprofen	SSL	~99	Malinowska et al. (2023)
2D TiO_2-GO		~7.5	~2.9			~97	
$ZnFe_2O_4$		~11	~1.5			~60	
TiO_2/γ-Fe_2O_3	TiO_2 nanoparticles on Fe_2O_3 edges	n.s	n.s	Dotarem	UVC	29	Alvarez-Aguiñaga et al. (2022)
TiO_2		(−)				39	
TiO_2/SiO_2@Fe_3O_4	Core (Fe_3O_4)-interlayer (SiO_2)-shell (TiO_2) Core (Fe_3O_4)/shell (TiO_2)	n.s	1.96	Ketamine	SSL	100[b]	Chen et al. (2022)
TiO_2/Fe_3O_4			n.s			32[b]	
TiO_2-P25						~100[b]	
Fe_3O_4/N-CXTi	Core (Fe_3O_4)/shell (N-CXTi) Core (Fe_3O_4)-interlayer (SiO_2)-shell (N-CXTi)	n.s	3.10	Acetaminophen	UV	~67.7	do Carmo Batista et al. (2022)
Fe_3O_4/SiO_2/N-CXTi			3.22			~99.2	
ZnO/γ-Fe_2O_3/Bentonite	γ-Fe_2O_3 and ZnO co-loaded on bentonite	n.s	n.s	Ciprofloxacin	SSL	93	Kamali et al. (2022)
ZnO/Bentonite		(−)				95	
Fe_3O_4/Bentonite		n.s				~45	
Fe_3O_4/$BiVO_4$/CdS	CdS on $BiVO_4$ and Fe_3O_4	n.s	n.s	Tetracycline	Vis	87.37	Xu et al. (2021)
$BiVO_4$		(−)	2.41			56.57	
CdS			2.23			23.18	
Ag/ZnO/$CoFe_2O_4$	$CoFe_2O_4$ covered with Ag/ZnO	n.s	3.21/3.43	Ibuprofen	UV	~65	Lenzi et al. (2021)
					SL	~21	
Ag/ZnO		(−)	2.95–3.29		UV	~90	
defective Fe_3O_4@SiO_2/d-TiO_2/Pt	Core (Fe_3O_4)-interlayer (SiO_2)-shell (TiO_2)	n.s	n.s	Carbamazepine	UV-Vis	~96	Dudziak et al. (2021)
					Vis	~55	
Fe_3O_4@SiO_2-TiO_2	Core (Fe_3O_4)-interlayer (SiO_2)-shell (TiO_2)	n.s	n.s	Nitrofurazone	UVA	~44	Smułek et al. (2021)
TiO_2-P25		(−)				~100	
Fe_3O_4@SiO_2/d-TiO_2-Pt/Cu	Core (Fe_3O_4)-interlayer (SiO_2)-shell (TiO_2-Pt/Cu)	n.s	n.s	Nitrophenol	UV-Vis	~88	Bielan et al. (2021)
TiO_2		(−)				~9	
Fe_3O_4@SiO_2/defective TiO_2-Pt/Cu	Core (Fe_3O_4)-interlayer (SiO_2)-shell (TiO_2-Pt/Cu)	n.s	2.75	Phenol	UV-Vis	22	Bielan et al. (2020)
					Vis	11	
Fe_3O_4@SiO_2/defective TiO_2		(−)	n.s		UV-Vis	20	
					Vis	8	
defective TiO_2		n.s	2.70		UV-Vis	40	
					Vis	13	
$MnFe_2O_4$@rGO@TiO_2	$MnFe_2O_4$ (core), rGO (first shell), TiO_2 (second shell)	33	n.s	Ofloxacin	SL	~80	Abdel-Wahed et al. (2020)
$MnFe_2O_4$@TiO_2		n.s				~46	
TiO_2		(−)				~62	
$MnFe_2O_4$		70				~29	
Fe_3O_4-TiO_2	Core (Fe_3O_4)-shell (TiO_2)	n.s	n.s	Phenol	UV	70	Lendzion-Bielun et al. (2020)
TiO_2-P25		(−)				100	

(Continued on following page)

TABLE 1 (*Continued*) Studies focused on the retrieval assistance role of the magnetic constituents of photocatalysts.

Photocatalyst	Magnetic composite morphology	Ms (emu/g)	Eg (eV)	Substrate	Light source	Performance[a] (%)	Ref.
Ag/Fe,N-TiO_2/Fe_3O_4@SiO_2	$CuFe_2O_4$ core coated with WO_3 and Ag	6.5	2.68	Ibuprofen, benzophenone-3	UV	~57	Khan et al. (2019a)
g-C_3N_4/TiO_2/Fe_3O_4@SiO_2		7.8	n.s			~100	
BiOBr@Fe_3O_4@SiO_2		8.5	2.74			>91	
$BiBr_{0.9}I_{0.1}$/Fe_3O_4@SiO_2		8	2.42			>94	
$BiOBr_{0.9}I_{0.1}$/Fe_3O_4@SiO_2	Fe_3O_4@SiO_2 (core@shell) distributed in $BiOBr_{0.9}I_{0.1}$ microstructures	35 (SPM)	2.42	Ibuprofen, benzophenone-3	Vis	>99	Fung et al. (2019)
$BiOBr_{0.9}I_{0.1}$		(–)	n.s			>99	
N-TiO_2@SiO_2@Fe_3O_4	Core (Fe_3O_4)-interlayer (SiO_2)-shell (N-TiO_2)	8.69 (SPM)	n.s	Ibuprofen, benzophenone-3, carbamazepine	Vis	>70[c]	Kumar et al. (2019)
Fe_3O_4/BiOBr/BC	BiOBr and Fe_3O_4 on BC external surface	5.20	n.s	Carbamazepine	Vis	95.51	Li S. et al. (2019)
Fe_3O_4/BiOBr		n.s				~70	
BiOBr		(–)				~90	
$NiFe_2O_4$/TiO_2/SiO_2 (TMAC)	$NiFe_2O_4$/TiO_2/SiO_2 (core-interlayer-shell) on activated carbon support	6.5 (SPM)	n.s	Tannic acid	UV	98.6	Li Y. et al. (2019)

[a]The performance of the different photocatalysts tested in each study are for the same experimental time unless otherwise specified.
[b]Different experimental times for each photocatalyst.
[c]Different experimental times for each contaminant.

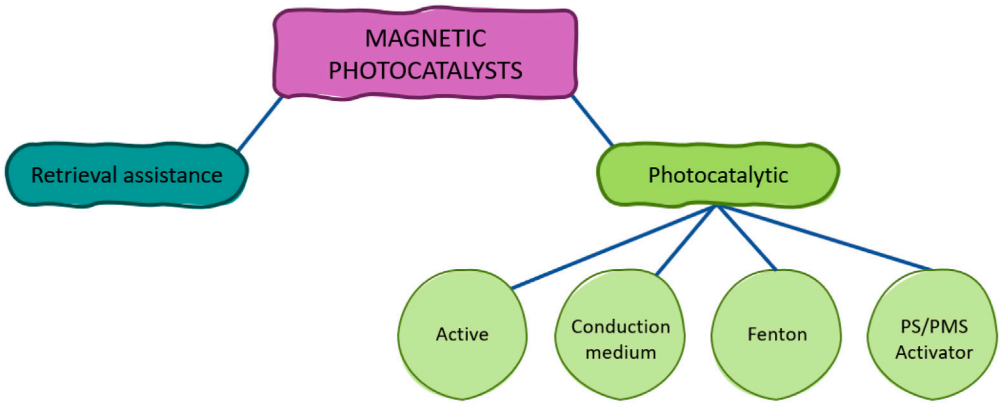

FIGURE 1
Schematic representation of the possible roles of the magnetic constituents of photocatalysts.

2 Roles of the magnetic component of photocatalysts on the degradation of organic pollutants

To give an updated picture of the application of magnetic photocatalysts in water treatment, literature in the field of magnetic photocatalysts for CECs degradation was surveyed for the last 6 years (2019–2024). Particularly, studies that use magnetic photocatalysts for dyes or microplastics degradation, inactivation of bacteria, or sewage disinfection have not been considered; on the other hand, works focused on the removal of phenolic compounds have been included, since they are typically used as model pollutants. Additionally, only studies that offer valuable insight about magnetic photocatalysts have been analyzed. The selected studies following these criteria have been categorized in Tables 1–5 according to the different roles of the magnetic constituent of the photocatalysts, which have been schematized in Figure 1. From these Tables, it can be noted that iron oxides (typically magnetite, Fe_3O_4) and ferrites

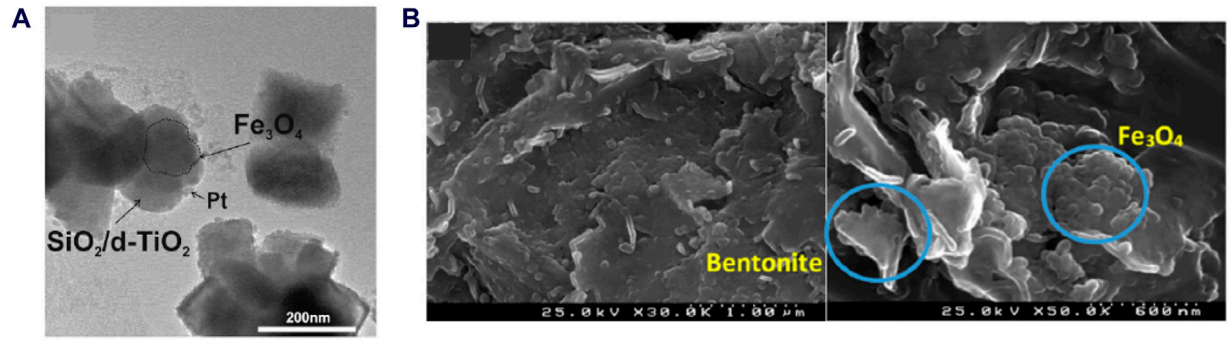

FIGURE 2
Images of photocatalysts where the magnetic constituent is located: **(A)** in the core (transmission electron microscopy, TEM); reprinted with permission from Dudziak et al. (2021), *J. Environ. Chem. Eng* (https://creativecommons.org/licenses/by/4.0/). or **(B)** deposited on the photocatalyst's surface (scanning electron microscope, SEM); reprinted with permission from Kamali et al. (2022), Molecules, (Creative Commons Attribution, CC BY, license https://creativecommons.org/licenses/by/4.0/).

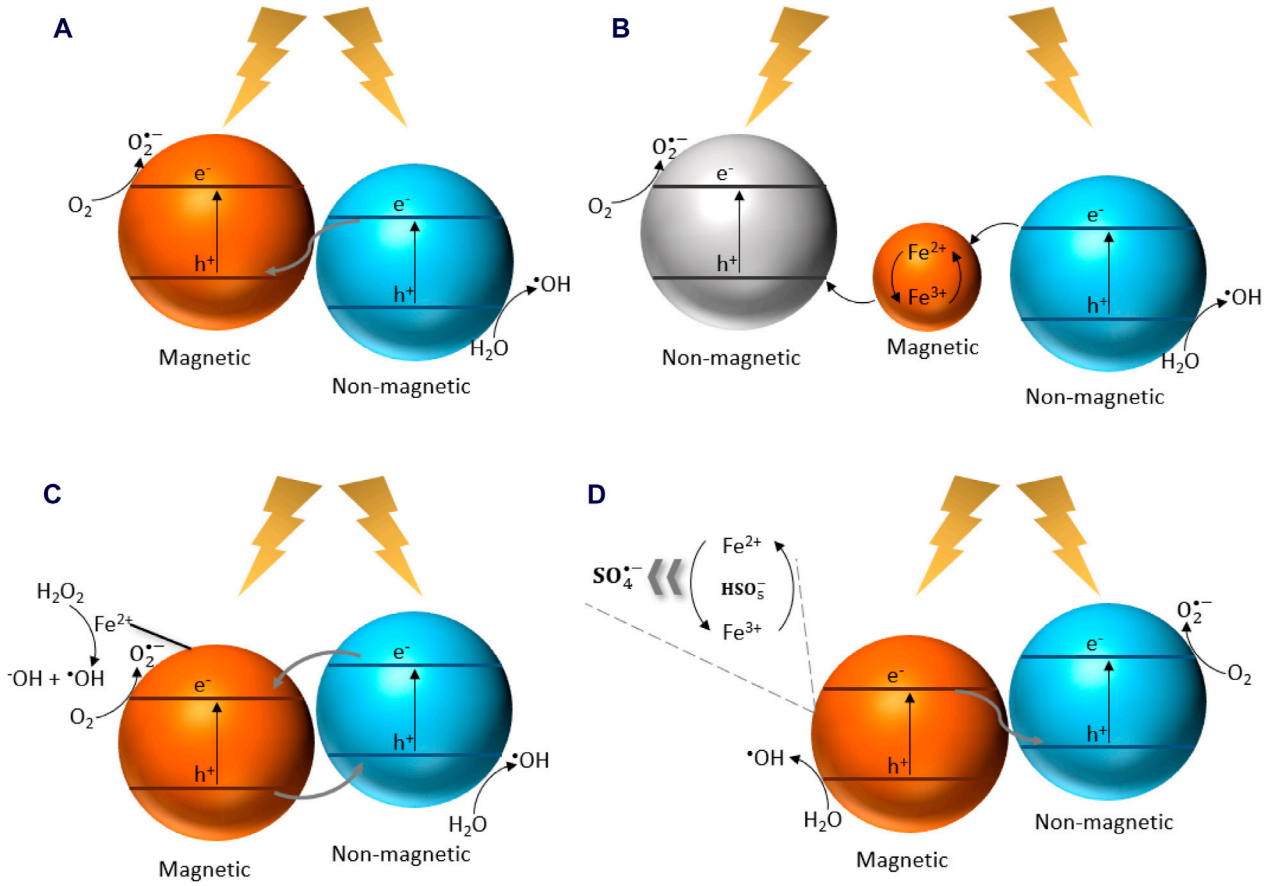

FIGURE 3
Schematics of the photocatalytic roles of the magnetic constituents of photocatalysts: **(A)** active catalyst, **(B)** conduction medium, **(C)** component of Fenton-like processes, and **(D)** PS/PMS activator.

(whose general formula is AFe_2O_4, where A is a divalent metal cation) are the prime candidates for being used as magnetic materials in magnetic photocatalysts (Singh et al., 2019; Belessiotis et al., 2022; Grzegórska et al., 2023). Thereby, magnetite and ferrites make up the photocatalysts that are employed in 44% and 48% of the studies surveyed in this work, respectively, which may substantiate the wide applicability of these magnetic materials in the synthesis of magnetic photocatalysts. In

TABLE 2 Studies focused on the active photocatalyst role of the magnetic constituents of photocatalysts.

Photocatalyst	Magnetic composite morphology	Ms (emu/g)	Eg (eV)	Substrate	Light source	Performance[a] (%)	Ref.
$NiO/NiFe_2O_4$	NiO is grown on $NiFe_2O_4$	n.s	n.s	2,4-dichlorophenol	Vis	~95	Shaheen et al. (2024)
$NiFe_2O_4$						~80	
$Ag\text{-}CuFe_2O_4@rGO$	$Ag\text{-}CuFe_2O_4$ on rGO sheets	n.s	2.03	4-nitrophenol	Vis	88.7	Sangeetha et al. (2024)
$Ag\text{-}CuFe_2O_4$			2.27			~37	
$CuFe_2O_4$			2.76			14.5	
$g\text{-}C_3N_4/Fe_3O_4$	Fe_3O_4 coated on $g\text{-}C_3N_4$ sheets	~19	1.7	Oxytetracycline	UVA	99.8	Mahmoudi et al. (2024)
$g\text{-}C_3N_4$		(–)	2.7			38.2	
Fe_3O_4		n.s	2.23			29.5	
$NiFe_2O_4/g\text{-}C_3N_4$	$NiFe_2O_4$ over $g\text{-}C_3N_4$ nanosheets	n.s	~2.6	2,4-dichlorophenol, bisphenol A	Vis	>40	Muhammad et al. (2024)
$g\text{-}C_3N_4$		(–)	~2.81			~10	
$TiO_2/CuFe_2O_4/Ag$	$CuFe_2O_4$ particles on TiO_2 surface	4.15	1.54	Naproxen	UV–Vis	92.56	Osanloo et al. (2024)
TiO_2		(–)	3.16			66.58	
$CuFe_2O_4$		11.2	1.48			37.8	
$MnFe_2O_4@Bi_{24}O_{31}Br_{10}/Bi_5O_7I$	Core ($MnFe_2O_4$)-shell ($Bi_{24}O_{31}Br_{10}/Bi_5O_7I$)	32.40	n.s	Levofloxacin, tetracycline, triclosan	SSL	>87	Liu M. et al. (2024)
$MnFe_2O_4$		74.38	1.74			~35	
$Fe_3O_4/ZnIn_2S_4$	Fe_3O_4 distributed on $ZnIn_2S_4$ surface	52.63	2.19	Gemifloxacin	SSL	94.1	Sun et al. (2024)
$ZnIn_2S_4$		(–)	2.43			85.5	
Fe_3O_4		82.25	1.92			10.13	
$CMCD\text{-}TiO_2@Fe_3O_4@RGO$	RGO encapsulated by nanoparticles	7.83	1.75	Tetracycline	Vis	83.3	Liu Z. et al. (2024)
$TiO_2@Fe_3O_4@RGO$		9.42	n.s			~70	
$TiO_2@Fe_3O_4$		n.s	2.14			~62	
TiO_2		(–)	3.20			~25	
$Ba_{0.5}Sr_{0.5}TiO_3$	$Ba_{0.5}Sr_{0.5}TiO_3$ particles surrounded by $BaFe_{12}O_{19}$	(–)	2.91	Tetracycline hydrochloride	SSL	53	Han et al. (2023)
$BaFe_{12}O_{19}$		48.96	1.29			41	
$Ba_{0.5}Sr_{0.5}TiO_3/BaFe_{12}O_{19}$		4.79	2.57			82	
$NiFe_2O_4/Bi/Bi_2WO_6/Bi_5O_7I$	Bi and $NiFe_2O_4$ on Bi_2WO_6/BiOI microspheres	4.1	n.s	Norfloxacin	Vis	96.5	Jabbar et al. (2023)
$Bi/Bi_2WO_6/Bi_5O_7I$		(–)				~70	
Fe_3O_4	(–)	n.s	0.11	Tetrabromobisphenol A	UV	~80	Kisała et al. (2023)
Fe_3O_4 nanopowder			1.75			~82	
$MnZnFe_2O_4@Ag_3PO_4$	$MnZnFe_2O_4$ surface coated with Ag_3PO_4	25.6	2.10	Phenol	Vis	100	Huang et al. (2023)
$MnZnFe_2O_4$		n.s	1.89			18.3	
Ag_3PO_4		(–)	2.43			74.9	
$Sn_3O_4/SnFe_2O_4$	$SnFe_2O_4$ attached on Sn_3O_4 flowers	10	2.09	Ciprofloxacin	Vis	57	Jiang et al. (2022)
Sn_3O_4		(–)	2.62			22	
$SnFe_2O_4$		50	1.9			17	

(Continued on following page)

TABLE 2 (*Continued*) Studies focused on the active photocatalyst role of the magnetic constituents of photocatalysts.

Photocatalyst	Magnetic composite morphology	Ms (emu/g)	Eg (eV)	Substrate	Light source	Performance[a] (%)	Ref.
g-C_3N_4/$NiFe_2O_4$	$NiFe_2O_4$ distributed over g-C_3N_4 sheets	n.s	n.s	Cephalexin	Vis	99.3	Sharma et al. (2022)
g-C_3N_4		(−)	2.66			38.2	
$NiFe_2O_4$		n.s	2.5			44.3	
$ZnFe_2O_4$/$Bi_7O_9I_3$	Core ($Bi_7O_9I_3$)-shell ($ZnFe_2O_4$)	23.1	1.87	Levofloxacin, sulfadiazine sodium, tetracycline	Vis	>94[b]	Zhao et al. (2022)
$Bi_7O_9I_3$		(−)	2.20			>61[b]	
$ZnFe_2O_4$		61.1	n.s			>72[b]	
Ag_3PO_4/Fe_3O_4	Core (Fe_3O_4)-shell (Ag_3PO_4)	n.s	n.s	Diclofenac sodium	UVA	~57	Bortolotto et al. (2022)
					SL	~68	
Ag_3PO_4		(−)	2.45		UVA	~59	
					SL	~53	
Fe_3O_4		n.s	n.s		UVA	~1	
					SL	~0	
3D-TiO_2/magnetic BC dots	Magnetic BC dots on 3D-TiO_2 microspheres	30.3	n.s	Diazinon	SL	98.5	Zahedifar and Seyedi (2022)
3D-TiO_2		(−)				~30	
Magnetic BC dots		42.1				~13.8	
$Mn_{0.6}Zn_{0.4}Fe_2O_4$@ $Zn_{0.95}Mn_{0.05}S$	Core ($Mn_{0.6}Zn_{0.4}Fe_2O_4$)/ shell ($Zn_{0.95}Mn_{0.05}S$)	24.6	2.57	Phenol	Vis	100	Niu et al. (2022)
$Zn_{0.95}Mn_{0.05}S$		(−)	2.92			~58	
$Mn_{0.6}Zn_{0.4}Fe_2O_4$		n.s	1.90			~28	
$ZnFe_2O_4$/Bi^0-Bi_2MoO_6	Bi^0 and $ZnFe_2O_4$ on Bi_2MoO_6 microspheres	6.45	1.97	Tetracycline hydrochloride	Vis	86.32	Wang et al. (2021)
Bi^0- Bi_2MoO_6		(−)	2.32			~58	
$ZnFe_2O_4$		n.s	1.80			~52	
CeO_2-TiO_2/PANI/ $NiFe_2O_4$	TiO_2 dispersed on PANI layers; combined CeO_2 and $NiFe_2O_4$ on TiO_2/PANI	0.004 (SPM)	1.6	Tetracycline hydrochloride	Vis	~60	Xie et al. (2021)
CeO_2-TiO_2/$NiFe_2O_4$		n.s	1.8			~80	
CeO_2-TiO_2		(−)	2.4			~60	
Fe_3O_4/TiO_2	Fe_3O_4 coated with TiO_2	21	n.s	Nitrobenzene	UV	74	Kunarti et al. (2021)
TiO_2		(−)	n.s			55	
Ag-$CuFe_2O_4$@WO_3	$CuFe_2O_4$ core coated with WO_3 and Ag	29.49	2.13	Gemfibrozil, tamoxifen	UV	~82	Sayadi et al. (2021)
$CuFe_2O_4$		62.57	n.s			~50	
TiO_2@$ZnFe_2O_4$/Pd	Core ($ZnFe_2O_4$)-shell (TiO_2/Pd)	27.28	n.s	Diclofenac	SL	86.1	Ahmadpour et al. (2020)
TiO_2@$ZnFe_2O_4$		37.32				~73	
$ZnFe_2O_4$		42.57				~49	
$CoFe_2O_4$/Ag_2MoO_4	Ag_2MoO_4 on $CoFe_2O_4$ nanosheets	38.16	2.15–2.60	Benzyl alcohol	Vis	82	Ghobadifard et al. (2020)
$CoFe_2O_4$		48.85	1.34			12	
Ag_2MoO_4		(−)	3			42	

(Continued on following page)

TABLE 2 (*Continued*) Studies focused on the active photocatalyst role of the magnetic constituents of photocatalysts.

Photocatalyst	Magnetic composite morphology	Ms (emu/g)	Eg (eV)	Substrate	Light source	Performance[a] (%)	Ref.
Bi_2WO_6-FeO_x	FeO_x on Bi_2WO_6 microspheres	6.7	2	Norfloxacin	LISL	~100	Karbasi et al. (2019)
Bi_2WO_6		(–)	2.6			~90	

[a]The performance of the different photocatalysts tested in each study are for the same experimental time unless otherwise specified.
[b]Different experimental times for each contaminant.

TABLE 3 Studies focused on the conduction medium role of the magnetic constituents of photocatalysts.

Photocatalyst	Magnetic composite morphology	Ms (emu/g)	Eg (eV)	Substrate	Light source	Performance[a] (%)	Ref.
g-C_3N_4/BiOBr/Fe_3O_4	BiOBr distributed on g-C_3N_4 nanosheets; Fe_3O_4 adhered on BiOBr and g-C_3N_4	~20	2.57	Tetracycline	SSL	96	Preeyanghaa et al. (2022)
g-C_3N_4/BiOBr		(–)	2.84			~88	
CdS/Fe_3O_4/TiO_2	Fe_3O_4 and CdS integrated with TiO_2 particles	2.5	2.84	Ibuprofen	Vis	94.2	Zhou et al. (2020)
CdS/TiO_2		(–)	2.76			73.6	

[a]The performance of the different photocatalysts tested in each study are for the same experimental time.

the upcoming subsections, the most commonly used magnetic materials and their possible roles are presented and discussed. Particularly, the function of the photocatalyst's magnetic components in the retrieval assistance is outlined in Section 2.1, whereas Section 2.2 elaborates on the different photocatalytic roles that these constituents could perform.

2.1 Improved separation and recovery of photocatalysts

The primary focus of compositing photocatalysts with magnetic materials lies in facilitating their recovery after use. Table 1 presents the surveyed studies that solely exploit the retrieval assistance function of the photocatalyst's magnetic constituents. Particularly, it encompasses studies that either do not demonstrate an enhancement in the pollutant removal with the inclusion of magnetic materials in the photocatalyst, or do not point out any photocatalytic role of the magnetic components.

According to Table 1, Fe_3O_4 is the predominant magnetic material used for photocatalyst retrieval in the vast majority of the research works. More specifically, about 67% of the selected studies employed Fe_3O_4 as magnetic source, while ~22% of works have reported compositing photocatalysts with ferrites. Additionally, it can be noticed that TiO_2 has been extensively utilized for degrading a wide variety of organic pollutants. This fact may derive from the appealing features of this photocatalysts, such as high photocatalytic activity and chemical stability, environmental friendliness, low-cost, corrosion resistance, and non-toxicity (Dharma et al., 2022; Sepahvand et al., 2022). When TiO_2 serves as the photocatalytic component, the composite typically has a core-shell structure as deduced from Table 1, where the magnetic material constitutes the core and is encapsulated in a TiO_2 shell. In most of these studies, a silicon dioxide (SiO_2) interlayer is introduced between the magnetic core and TiO_2 to prevent their interaction and assist the stability of the magnetic core (Khan et al., 2019a; Kumar et al., 2019; Sepahvand et al., 2022). An example of the core-interlayer-shell structure is shown in Figure 2A, where the coating of the magnetic core by a SiO_2/TiO_2 shell can be distinguished. Alternatively, the magnetic constituent can be loaded on the material surface. Figure 2B depicts this configuration, showing Fe_3O_4 nanoparticles growing on the surface of bentonite.

It is worth highlighting that for core-shell structures the thickness of the photocatalysts layer (shell) strongly impacts the efficiency of the photocatalytic and magnetic recovery stages. Specifically, the thickness of the photocatalyst layer should alter the diffusion layer, thus modifying the photocatalytic activity; moreover, the thicker the photocatalyst layer the worse magnetization of the material (Abdel-Wahed et al., 2020). In this regard, it is interesting to note that although the magnetic photocatalysts can be magnetically retrieved, they exhibit lower saturation magnetization than pure magnetite or ferrite, as evidenced in Table 1. Such magnetism reduction of the composite is caused by the presence of non-magnetic materials (Xu et al., 2021; Yilmaz et al., 2022). Hence, it is observed regardless of the type of photocatalytic semiconductor or the location of the magnetic material in the composite, that is in its core (for core-shell structures) or on the surface (when magnetic components are deposited on the material). For instance, Xu et al. (2021) found that the saturation magnetization (Ms) was drastically decreased when Fe_3O_4 (Ms = 85.9 emu/g) was composited with non-magnetic CdS and $BiVO_4$ in the Fe_3O_4/$BiVO_4$/CdS photocatalyst (Ms = 10.3 emu/g). Similarly, Kumar et al. (2019) reported that the coating of N-TiO_2 and SiO_2 on

TABLE 4 Studies focused on the synergy between photocatalysis and Fenton-like oxidation due to the magnetic constituents of photocatalysts.

Photocatalyst	Magnetic composite morphology	Ms (emu/g)	Eg (eV)	Substrate	Light source	Performance[a] (%)	Ref.
Cd/CdS-$ZnFe_2O_4$/α-Fe_2O_3	$ZnFe_2O_4$/α-Fe_2O_3 nanoparticles on Cd/CdS surface	n.s	n.s	Tetracycline	Vis	91.72	Zhu et al. (2024)
Cd/CdS-$ZnFe_2O_4$/α-Fe_2O_3 (w/o + H_2O_2)						76.09	
CdS/Fe_3O_4@NGAM/N-TiO_2	Inner (CdS), middle (Fe_3O_4), and outer (N-TiO_2) layers of NGAM	27.67	2.71	Bisphenol A, tetracycline hydrochloride	Vis	96[b]	Wang et al. (2024b)
CdS@NGAM/N-TiO_2		(−)	n.s			<83[b]	
BC/FeOOH	Layer of FeOOH nanoneedles on BC	n.s	n.s	Tetracycline	Vis	92	Xue et al. (2024)
BC/FeOOH (w/o H_2O_2)						70	
FeOOH		n.s	2.04			~72	
FeOOH (w/o H_2O_2)						~48	
Fe_3O_4@PAA/SBA15	n.s	n.s	n.s	Carbamazepine	LED	~72	González-Rodríguez et al. (2024)
				Bisphenol A		~92	
				Estrone, 17a-ethinylestradiol		~100	
				Estradiol		~94	
Ag/s-(Co_3O_4/$NiFe_2O_4$)	$NiFe_2O_4$ and Ag loadaded on Co_3O_4 particles	8.34 (SPM)	n.s	Tetracycline	Vis	~75	Kumar et al. (2022)
Co_3O_4/$NiFe_2O_4$		14.23 (SPM)				~8	
Co_3O_4		(−)	2.15			~3	
$NiFe_2O_4$		n.s	2.20			~8	
$CoFe_2O_4$/SiO_2/TiO_2	Core ($CoFe_2O_4$)-interlayer (SiO_2)-shell (TiO_2)	3.52	3.06	2,4-dinitrotoluene	UV	88.5	Sepahvand et al. (2022)
$CoFe_2O_4$/TiO_2		n.s	n.s			70.68	
TiO_2-P25		(−)	3.2			60.02	
WO_3/Fe_3O_4	WO_3 on Fe_3O_4 support	43.2	n.s	Thiacloprid	SSL	66.1	Banic et al. (2019)
WO_3		(−)				~31	
Fe_3O_4		5.4				~28	
Fe_3O_4/ZnO	Fe_3O_4 and ZnO mixed in the aggregates	4.3 (SPM)	n.s	Sulfamethoxazole, trimethoprim, erythromycin and roxithromycin	UVA	100	Fernández et al. (2019)

[a]The performance of the different photocatalysts tested in each study are for the same experimental time unless otherwise specified.
[b]Different experimental times for each contaminant.

Fe_3O_4 resulted in the considerable reduction of the saturation magnetization of N-TiO_2@SiO_2@Fe_3O_4 (Ms = 8.69 emu/g) in comparison to pure Fe_3O_4 (Ms = 43.94 emu/g). Despite the evidenced magnetism reduction, Xu et al. (2021) demonstrated the successful retrieval of the photocatalyst by applying an external magnetic field. Thereby, although the reduction in the saturation magnetization does not hinder the magnetic separation of the photocatalyst, it involves an increase in the time required to fulfill such retrieval (Fuziki et al., 2021). Regarding the time to accomplish the magnetic recovery of the catalysts, Kumar et al. (2019) experimentally demonstrated that after 25 min the separation efficiency under a magnetic field was 97%, thus supporting the attractive possibilities of the magnetically facilitated recovery of photocatalysts.

Apart from having magnetic responsiveness, some of the photocatalysts gathered in Table 1 are also superparamagnetic. Particularly, Fung et al., 2019 and Kumar et al. (2019) highlighted the superparamagnetic behavior of their $BiOBr_{0.9}I_{0.1}$/Fe_3O_4@SiO_2 and N-TiO_2@SiO_2@Fe_3O_4 photocatalysts, respectively. The superparamagnetic nature is revealed by their S-shaped magnetization curves, which are distinctive of superparamagnetic materials (Zimmermann, G. et al., 2003; Abdel-Wahed et al., 2020).

TABLE 5 Studies focused on the coupling between PS/PMS and photocatalysis oxidation.

Photocatalyst	Magnetic composite morphology	Ms (emu/g)	Eg (eV)	Substrate	Light source + PS/PMS	Performance[a] (%)	Ref.
Co_3O_4@P-doped g-C_3N_4/α-Fe_2O_3	Co_3O_4 over P-doped g-C_3N_4/α-Fe_2O_3 surface	~0.021	1.74	Bisphenol-A	Vis/PS	99.3	Rangaraj et al. (2024)
Co_3O_4@P-doped g-C_3N_4		(–)	1.82			91	
Fe_3O_4	(–)	n.s	2.61	2,4-dichlorophenol	Vis/PMS	100	Wang et al. (2024a)
					Vis	~15	
MIL-53(Fe) derived Fe_3O_4@C	Fe_3O_4 nanoparticles interconnected by carbon networks	37.74	1.3	Salicylic acid	UVC/PS	95.45	Priyadarshini et al. (2024)
					UVC	12.35	
MOF-derived $CoFe_2O_4$/FeS_2	FeS_2 distributed around octahedral MOF-derived $CoFe_2O_4$	~52	n.s	Tetracycline	Vis/PS	85.4	Hao et al. (2024)
FeS_2		(–)	1.22			68	
MOF-derived $CoFe_2O_4$		n.s	2.52			70	
MOF-derived $CoFe_2O_4$/FeS_2		~52	n.s		Vis	31.4	
AgBr/BiOBr/Fe_3O_4	Fe_3O_4 on AgBr/BiOBr surface	4.54	2.88	Carbamazepine	Vis/PMS	96.84	Tao et al. (2024)
AgBr/BiOBr		(–)	2.90			~85	
Fe_3O_4		81.64	n.s			~25	
$CuFe_2O_4$/MnO_2	Core ($CuFe_2O_4$)-shell (MnO_2)	~4.8	1.44	Tetracycline, 2-nitrophenol, ceftriaxone sodium	Vis/PMS	>85	Song et al. (2024)
$CuFe_2O_4$		~12.5	1.60			>68	
TiO_2/Ti_3C_2/$MnFe_2O_4$	$MnFe_2O_4$ in TiO_2/Ti_3C_2	5	2.99	Carbamazepine and Ibuprofen	SSL/PMS	100[b]	Grzegórska et al. (2023)
					SSL	~100	
TiO_2/Ti_3C_2		(–)	3			>96	
$MnFe_2O_4$		68	1.5			<15	
$SrTiO_3$/$BaFe_{12}O_{19}$	n.s	2.98	3.09	Tetracycline	Vis/PMS	96.1	Feng et al. (2023)
$BaFe_{12}O_{19}$		n.s	n.s			16.3	
$SrTiO_3$		(–)	2.84			69	
$SrTiO_3$/$BaFe_{12}O_{19}$		2.98	3.09		Vis	32	
$BaFe_{12}O_{19}$		n.s	n.s			~3	
$SrTiO_3$		(–)	2.84			19.3	
$ZnFe_2O_4$/A-MoS_2	$ZnFe_2O_4$ on A-MoS_2 nanosheets	13.49	n.s	Carbamazepine	Vis	<10	Zheng et al. (2023)
$ZnFe_2O_4$/A-MoS_2					Vis/PMS	100	
$ZnFe_2O_4$		75.26	1.75			38.4	
A-MoS_2		(–)	1.67			43.1	
ZnO@$CoFe_2O_4$@CNT	$CoFe_2O_4$ and ZnO deposited over MWCNT	28	2.3	Cefixime	UVC/PMS	100	Tian et al. (2023)
					UVC	46	
Spinel ferrite@g-C_3N_4	Spinel ferrite on planar g-C_3N_4	32	2.4	Biphenol A	UVC/PMS	100	Moradi et al. (2022)
					UVC	~58	
g-C_3N_4		(–)	2.8			~8	

(Continued on following page)

TABLE 5 (*Continued*) Studies focused on the coupling between PS/PMS and photocatalysis oxidation.

Photocatalyst	Magnetic composite morphology	Ms (emu/g)	Eg (eV)	Substrate	Light source + PS/PMS	Performance[a] (%)	Ref.
Fe_3O_4@CeO_2@ BiOI	Fe_3O_4 surface coated with CeO_2 and BiOI	20.2 (SPM)	1.46	Sulfamethoxadole	UVA/PMS	97	Kohantorabi et al. (2021)
					UVA	~78	
CeO_2@BiOI		—	n.s		UVA/PMS	~89	
					UVA	~80	
BiOCl@Fe_3O_4	n.s	n.s	n.s	Atenolol	SSL	38.5	Wu et al. (2019)
					SSL/PMS	70.2	

[a]The performance of the different photocatalysts tested in each study are for the same experimental time unless otherwise specified.
[b]Different experimental times for each contaminant.

Specifically, this type of materials exhibits low retentivity, and thus residual magnetic forces do not exist after removing the external magnetic field, which enables the quick redispersion of the photocatalyst once the magnetic field is ceased (Moniriyan et al., 2021; Xie et al., 2021). Superparamagnetism occurs in ferromagnetic and ferrimagnetic nanoparticles when their diameter falls below a critical threshold, which ranges from 3 to 50 nm depending on the material (Marghussian, 2015; Gómez-Pastora et al., 2017b). Superparamagnetic materials are attractive for water treatment applications due to the reversibility of their magnetic interactions. As a result, in absence of magnetic fields these materials can be redispersed in the aqueous media. Thereby, the agglomeration of the photocatalysts, which causes the reduction of its surface area, is prevented, thus demonstrating the possibility of being reused (Khan et al., 2019b; Abdel-Wahed et al., 2020; Zhou et al., 2020).

The features of magnetic photocatalysts outlined throughout this subsection support the promising prospects of integrating semiconductors with magnetic materials, since the resulting composite can be efficiently recovered by magnetic means. However, when designing magnetic photocatalysts it is crucial to take into account not only their easy recovery after use but also their efficiency to degrade the target pollutants. The photocatalyst's magnetic constituents could have different effects on the contaminant removal. Thereby, they could either enhance the efficiency of photodegradation, which will be comprehensively discussed in the next section, or negatively affect it. In this regard, Smułek et al. (2021) and Lendzion-Bielun et al. (2020) conducted comparative studies on the ability of Fe_3O_4@SiO_2-TiO_2 and Fe_3O_4-TiO_2, respectively, to degrade target contaminants against TiO_2-P25. It is noteworthy that Smułek et al. (2021) and Lendzion-Bielun et al. (2020) synthesized the TiO_2 of their composites, which could compromise the direct comparison with TiO_2-P25 since they are different materials. Furthermore, the differences in the performance of the composite material could be also attributed to a lower catalyst concentration than that used for pristine catalyst. Despite the challenges for this comparison, Smułek et al. (2021) reported that while TiO_2-P25 was able to almost completely remove nitrofurazone in 60 min, only 44% of the pollutant was degraded during the same time period using Fe_3O_4@SiO_2-TiO_2. On the other hand, Lendzion-Bielun et al. (2020) observed that 100% phenol conversion could be achieved using both TiO_2-P25 and Fe_3O_4-TiO_2. However, the former required 200 min and the later 300 min for achieving the same degradation. Although TiO_2-P25 demonstrated an efficient performance, Smułek et al. (2021) and Lendzion-Bielun et al. (2020) concluded that the easy separation of magnetic photocatalysts from the treated media by applying magnetic fields supports the interest in their use for pollutant degradation. Hence, although pristine TiO_2 could yield a higher conversion of the contaminant, its challenging recovery after use ultimately hinders its practical application.

Overall, the main interest in integrating semiconductors with magnetic materials lies in enhancing the recovery of the resulting composite after use. In this context, the attractive potential of the magnetically assisted photocatalysts recovery overcomes the possible reduction in degradation efficiency of magnetic photocatalysts. According to the studies herein surveyed, Fe_3O_4 stands out as the predominantly used magnetic material when the purpose of incorporating magnetic materials into the photocatalysts is solely to enhance their retrieval. In this regard, efficient magnetic separation has been demonstrated despite the lower saturation magnetization of the composite photocatalyst compared to the pure magnetic materials. Additionally, magnetic photocatalysts exhibiting a superparamagnetic behavior have been synthesized, which is especially attractive for the successful re-use of the photocatalysts after their magnetic retrieval.

2.2 Enhanced activity of photocatalytic materials with magnetic components

As it has been widely highlighted in the literature, the introduction of magnetic components to the photocatalysts make it possible their easy separation from the treated medium. However, the magnetic constituents not only play a pivotal role in facilitating the recovery of the photocatalyst, but they could also be involved in the photodegradation of contaminants. Recognizing the different photocatalytic-based roles the magnetic materials that constitute the composite can play in the process may be of paramount interest for

enhancing the efficiency of the degradation of pollutants. Therefore, in this section, the roughly classified as photocatalytic functions that the magnetic constituents can fulfill, which include (i) active catalyst, (ii) conduction medium, (iii) component of Fenton-like processes and (iv) persulfate (PS)/PMS activator, are presented and discussed. A general representation of these functions is depicted in Figure 3. It can be noted that for all roles the magnetic photocatalyst comprises at least one material of non-magnetic character (i.e., the semiconductor) and a magnetic material. The magnetic constituent can be involved in the formation of radicals through two different strategies. On the one hand, it can generate $^{\bullet}OH$ or $O_2^{\bullet-}$ radicals when it acts as active catalyst (Figure 3A), component of Fenton-like process (Figure 3C) or PS/PMS activator (Figure 3D). Alternatively, the magnetic material can also serve as conduction medium (Figure 3B) of e^- between semiconductors; in this scenario, the semiconductors are the photocatalyst's constituents responsible for the generation of radicals. An in-depth description of the different photocatalytic roles that magnetic materials can exhibit is provided in the following subsections.

2.2.1 Magnetic constituent as active catalyst

When the magnetic components that constitute the photocatalyst can be photoexcited to generate e^- and h^+ in their conduction (CB) and valence (VB) bands, respectively, and as a result the degradation efficiency is enhanced, they act as photocatalysts (Table 2). For instance, Wang et al. (2021), Zhao et al. (2022) and Ahmadpour et al. (2020) reported that $ZnFe_2O_4$ was able to yield degradation efficiencies exceeding 50% of the target pollutants; similarly, Sayadi et al., 2021 stated that $CuFe_2O_4$ was able to degrade 47% of gemfibrozil. According to Table 2, which includes the studies where the magnetic component acts as photocatalyst, ferrites are extensively used as magnetic materials. This observation may be in line with the exploitation of ferrite photocatalysts for the removal of organic pollutants that has been reported in the literature (Gupta et al., 2020). Particularly, ferrites have garnered interest as photocatalysts due to their narrow band gap, enabling them to harness visible light. Additionally, ferrites have a tunable band gap since depending on the ferrite (e.g., Zn-, Mn-, Co-ferrite, etc.) they exhibit a different band gap (<2.5 eV) and band positions (Ma and Liu, 2021; Cheng et al., 2023; Zheng et al., 2024).

Additionally, ferrites can be composited with semiconductor materials, which results in an improved photocatalytic performance (Casbeer et al., 2012; Kefeni and Mamba, 2020; Wu and Song, 2023). In this context, the magnetic materials generally reduce the band gap and/or inhibit the recombination of the photogenerated e^-/h^+ pairs mainly due to the formation of Z- or S-scheme heterojunctions with the semiconductors. Hence, the photocatalytic activity typically enhances when magnetic materials are introduced to the composite and work as photocatalysts. For instance, Wang et al. (2021) reported that the efficiency to degrade tetracycline hydrochloride upon visible light irradiation of the $ZnFe_2O_4/Bi^0$-Bi_2MoO_6 composite they prepared was around 87%, which is considerably higher than that for pure Bi^0-Bi_2MoO_6 (52%). They explained that the introduction of $ZnFe_2O_4$ decreases the band gap (from 2.32 eV for Bi^0-Bi_2MoO_6 to 1.97 eV $ZnFe_2O_4/Bi^0$-Bi_2MoO_6), broadens the spectral absorption range of the photocatalyst, and results in the formation of a Z-scheme heterojunction to facilitate the charge separation. Particularly, they suggested that both Bi_2MoO_6 and $ZnFe_2O_4$ where excited under visible light irradiation to produce e^- and h^+. The photogenerated e^- of Bi_2MoO_6 could migrate to the nano-Bi^0 and $ZnFe_2O_4$. Hence, nano-Bi^0 and $ZnFe_2O_4$ can reduce O_2 to $O_2^{\bullet-}$, which is involved in tetracycline degradation. They explained that the h^+ of $ZnFe_2O_4$ capture the e^- of Bi_2MoO_6 that migrate to $ZnFe_2O_4$ surface. Thereby, the recombination of the own $ZnFe_2O_4$'s e^-/h^+ pairs is inhibited and thus, highly reducing e^- are retained in $ZnFe_2O_4$'s CB. On the other hand, the h^+ of Bi_2MoO_6 produce $^{\bullet}OH$, which also takes part in the removal of the pollutant. They concluded that the formation of the Z-scheme heterojunction between $ZnFe_2O_4$ and Bi_2MoO_6 promotes the separation of the photogenerated e^-, which ultimately led to an enhancement of the catalyst's activity. Similarly, Sharma et al. (2022) found that the efficiency in the degradation of cephalexin under visible light irradiation increased from 38.2% for pristine g-C_3N_4 to 99.3% for g-C_3N_4/$NiFe_2O_4$, which form a S-scheme heterojunction. They ascribed this observation to the fact that the compositing of g-C_3N_4 and $NiFe_2O_4$ reduces recombination, improves visible light activity and charge migration on the heterojunction. According to their proposed catalytic mechanism, upon light irradiation the e^- of both g-C_3N_4 and $NiFe_2O_4$ are excited to generate e^-/h^+ pairs. Then, the e^- of $NiFe_2O_4$'s CB can be transferred to the g-C3N4's VB through an S-scheme mechanism. Thereby, the protected e^- in g-C_3N_4 and h^+ in $NiFe_2O_4$'s VB are involved in the production of the active species ($O_2^{\bullet-}$ and $^{\bullet}OH$ radicals) for degrading the target antibiotic.

2.2.2 Magnetic constituent as conduction medium

The magnetic components can also work as a conduction medium for the photogenerated e^- so that they are effectively transferred between the semiconductors that constitute the photocatalytic composite. As noticed from Table 3, only Zhou et al. (2020) and Preeyanghaa et al. (2022) have raised this role of the photocatalyst's magnetic constituent. More specifically, Zhou et al. (2020) and Preeyanghaa et al. (2022) reported that Fe_3O_4 can serve as an electron mediator to foster the building of Z-scheme heterojunctions. This role stems from the fact that Fe^{3+} and Fe^{2+} in Fe_3O_4 can act as recombination centers to capture photogenerated e^- and h^+ (Zhou et al., 2020). Particularly, Zhou et al. (2020) indicated that the following reactions could be involved when Fe_3O_4 acts as conduction medium:

$$\mathbf{F_3O_4\,(e^-) + Fe^{3+} \rightarrow Fe^{2+}} \quad (1)$$

$$\mathbf{F_3O_4\,(h^+) + Fe^{2+} \rightarrow Fe^{3+}} \quad (2)$$

In this context, Preeyanghaa et al. (2022) proposed a photocatalytic reaction mechanism for g-C_3N_4/BiOBr/Fe_3O_4 under simulated solar light irradiation that highlights the role of Fe_3O_4 as the conduction medium to transfer the CB e^- of BiOBr to the heterojunction interface; subsequently, these e^- are recombined with the VB h^+ of g-C_3N_4. This way, the recombination of the photogenerated e^-/h^+ pairs in BiOBr and g-C_3N_4 is avoided, thus leading to the accumulation of h^+ in the VB of BiOBr and e^- in the CB of g-C_3N_4. These accumulated h^+ and e^- are involved in the production of $^{\bullet}OH$ and $O_2^{\bullet-}$, respectively, which could effectively degrade the target pollutant, that is, tetracycline (Zhou et al., 2020; Preeyanghaa et al., 2022). Similarly, Zhou et al. (2020) also pointed out the role of Fe_3O_4 as electron mediator in the CdS/Fe_3O_4/TiO_2 composite they prepared. Zhou et al. (2020) explained that Fe_3O_4

could boost the formation of the Z-scheme heterojunction, thus avoiding the recombination of the photogenerated e^-/h^+ pairs. Particularly, they suggest that the e^- and h^+ in the TiO_2's CB and CdS's VB, respectively, would be transferred to Fe_3O_4 and recombined. Thereby, the h^+ on the VB of TiO_2 and the e^- on the CB of CdS could be involved in the generation of $^{\bullet}OH$, which can oxidize the target pollutant. Although the works by Preeyanghaa et al. (2022) and Zhou et al. (2020) offer valuable insights, there is a need for comprehensively elucidating the mechanism underlaying the conduction medium role of the magnetic constituents, since the scarcity of research in that field causes that a complete picture about this role cannot be accurately provided.

2.2.3 Magnetic constituent as element of Fenton-like processes

The Fe ions that constitute the magnetic materials can be also involved in Fenton reactions, leading to the synergistic degradation of contaminants due to photocatalytic and Fenton oxidation. Combining Fenton reaction with light irradiation results in photo-Fenton processes, which exhibit higher degradation rate compared to classical Fenton processes (Jiang Y. et al., 2022; Machado et al., 2023; Bule Možar et al., 2024). Particularly, light irradiation enhances the process performance by increasing the generation of $^{\bullet}OH$ radicals through the decomposition of H_2O_2 and promoting the regeneration of Fe^{2+} ions (O'Dowd and Pillai, 2020; Ganiyu et al., 2022; Machado et al., 2023; Wu et al., 2023). Thereby, the photo-Fenton process involves the following reactions:

$$Fe^{2+} + H_2O_2 \rightarrow Fe^{3+} + OH^- + OH^{\bullet} \quad (3)$$

$$Fe^{3+} + H_2O + h\nu \rightarrow Fe^{2+} + OH^{\bullet} + H^+ \quad (4)$$

$$H_2O_2 + h\nu \rightarrow 2\,OH^{\bullet} \quad (5)$$

Table 4 collects studies that investigate the degradation of pollutants by coupling semiconductor photocatalysis with the photo-Fenton process involving the magnetic constituent of the photocatalysts. It can be noticed that while visible light is typically used in these systems, UVA irradiation has also been employed as the light source. Moreover, Fe_3O_4 is a magnetic material added in the composite when the Fenton-like process contributes to the pollutants degradation, together with photocatalysis. Although Fe_3O_4 is a traditional Fenton counterpart, photocatalysts containing ferrites, such as $CoFe_2O_4$, can also be involved in this process for generating ·OH radicals as it has been suggested (Preeyanghaa et al., 2022; Sepahvand et al., 2022). The use of magnetic photocatalyst in the photo-Fenton removal of contaminants was reported by Banic et al. (2019), who investigated the efficiency for degrading thiacloprid of WO_3/Fe_3O_4 under simulated solar radiation in the presence and absence of H_2O_2. They found that the pollutant removal increased from 5% (WO_3/Fe_3O_4) to 65% (WO_3/Fe_3O_4/H_2O_2) when H_2O_2 was present. They reasoned that besides the influence of the coupling effect of WO_3 and Fe_3O_4, the heterogeneous photo-Fenton process also affects the degradation efficiency. On a similar note, Sepahvand et al. (2022) proposed that the magnetic constituent of their $CoFe_2O_4$/TiO_2/SiO_2 photocatalyst could also take part in the degradation of 2,4-dinitrotoluene. Particularly, they proposed a mechanism, where apart from the photogenerated e^- and h^+ in TiO_2, $CoFe_2O_4$ could be also involved in the generation of $^{\bullet}OH$ radicals to degrade the pollutant by the reaction of their Fe^{2+} ions with H_2O_2. However, exploiting the Fenton-implication role of $CoFe_2O_4$ in the photocatalyst prepared by Sepahvand et al. (2022) may prove challenging due to its core-interlayer-shell configuration. More specifically, $CoFe_2O_4$ is coated by TiO_2@SiO_2 and constitutes the photocatalyst's core. Hence, the photocatalyst's magnetic constituent in the study of Sepahvand et al. (2022) is not in contact with H_2O_2. This fact contrasts with the work by Banic et al. (2019) where H_2O_2 was decomposed on the surface of the iron oxide. On the other hand, it should be emphasized that some studies presented in Table 4 examine how the solution pH impacts the degradation efficiency of pollutants. This investigation may derive from the fact that Fenton's reactions are reported to be affected by the pH of the media, and thus, identifying the conditions that yield an optimum system performance is of utmost importance (Jung et al., 2009; Chen et al., 2023). For instance, Xue et al. (2024) explored the degradation of tetracycline using the Biochar/FeOOH photocatalysts at several pH values in the range from 3 to 11. They found that increasing the pH resulted in an enhancement of tetracycline degradation (92% for pH = 9 and 11, and ~82% for pH = 3). Particularly, Xue et al. (2024) ascribed the diminished degradation efficiency under acidic conditions to the inhibition of the Fe^{2+}/Fe^{3+} cycle by H^+. Another key insight from the study by Xue et al. (2024) is ability of the magnetic component (FeOOH) to degrade the pollutant under light exposure when it is not composited with the biochar. Specifically, Xue et al. (2024) reported degradation efficiencies for FeOOH of 48% and 72% in absence and presence of H_2O_2, respectively. From Table 4, it can be noted that this ability for removing tetracycline is comparable to that reported by Kumar et al. (2022), who obtained 75% removal of tetracycline in a photo-Fenton process that uses *in situ* generated H_2O_2 and Ag/s-(Co_3O_4/$NiFe_2O_4$) as photocatalyst. The similar photodegradation ability of FeOOH compared to other photocatalysts evidences the potential of FeOOH to be used alone for the removal of target contaminants.

2.2.4 Magnetic constituent as activator of persulfate or peroxymonosulfate

The above-mentioned photocatalytic-based roles of the magnetic materials are related to traditional AOPs relaying on $^{\bullet}OH$ radicals. However, AOPs based on $SO_4^{\bullet-}$ radicals have also been considered an effective oxidation method for the degradation of pollutants from aqueous matrices (Yu et al., 2020; Li et al., 2022). In particular, $SO_4^{\bullet-}$ possesses longer half-life (30–40 μs), high redox potential (2.5–3.1 V), and the possibility of being applied in a wide range of pH (2–11) compared to $^{\bullet}OH$ radicals. $SO_4^{\bullet-}$ is produced from the activation of PS ($S_2O_8^{2-}$) or PMS (HSO_5^-), which is achieved through several strategies, including, ultraviolet light, transition metal ions, metal oxides or e^-/h^+ pairs from the photocatalyst (Wu et al., 2019; Kohantorabi et al., 2021; Moradi et al., 2022). Examples of the reactions that take place for the activation PS or PMS by light (Eqs 6, 7) and e^- from the photocatalyst (Eqs. 8, 9) are given below:

$$HSO_5^- + h\nu \rightarrow SO_4^{\bullet-} + OH^{\bullet} \quad (6)$$

$$SO_4^{\bullet-} + H_2O \rightarrow SO_4^{2-} + OH^{\bullet} + H^+ \quad (7)$$

$$\text{Photocatalyst} + h\nu \rightarrow e^- + h^+ \quad (8)$$

$$HSO_5^- + e^- \rightarrow SO_4^{\bullet-} + OH^- \quad (9)$$

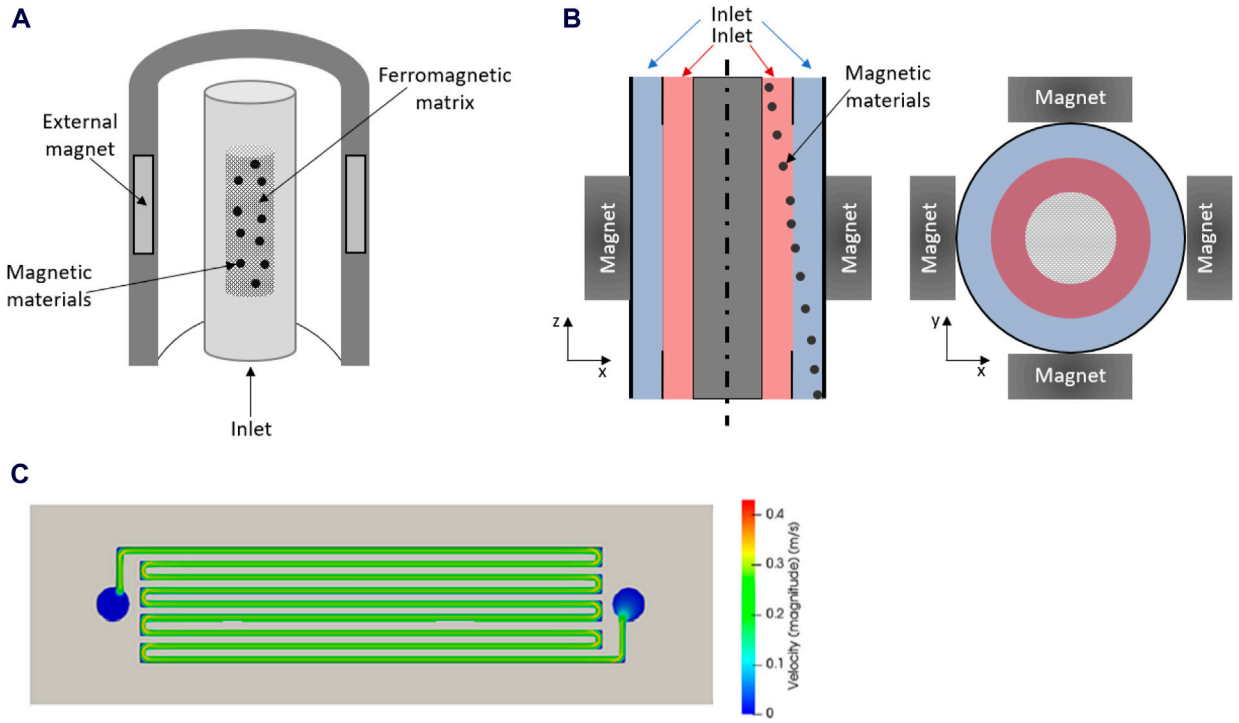

FIGURE 4
Schematic diagram of **(A)** HGMS, and **(B)** OGMS with the quadrupole magnetic configuration (Adapted from González-Fernández et al. (2021), *Ind. Eng. Chem. Res.* https://creativecommons.org/licenses/by/4.0/). **(C)** Example of velocity fields predicted by CFD simulations in a serpentine channel; Reprinted from Saif et al. (2024), *Desalination* (https://creativecommons.org/licenses/by-nc-nd/4.0/).

On the other hand, PMS activation through Fe could undergo reactions 10 and 11, which are analogous for other transition metals such as Mn and Co (Kohantorabi et al., 2021; Grzegórska et al., 2023). It is worth pointing out that although these reactions do not directly involve light they have been here included since transition metals constitute the photocatalyst, and thus the reactions can occur in the photocatalytic system.

$$Fe^{3+} + HSO_5^- \rightarrow Fe^{2+} + SO_5^{\bullet-} + H^+ \quad (10)$$

$$Fe^{2+} + HSO_5^- \rightarrow Fe^{3+} + SO_4^{\bullet-} + OH^- \quad (11)$$

In this context, the activation of PMS or PS coupled to semiconductor photocatalysis has been reported (Table 5). For instance Grzegórska et al. (2023), Moradi et al. (2022), and Kohantorabi et al. (2021) proposed a mechanism for the photocatalytic degradation of a different contaminant over TiO_2/Ti_3C_2/$MnFe_2O_4$/PMS, SCF/g-C_3N_4/PS/UVC, Fe_3O_4/CeO_2/BiOI/UVA/PMS processes, respectively. Particularly, Grzegórska et al. (2023) posed that PMS could be activated by Mn and Fe in their system and determined the rate-limiting steps in the PMS activation process. On the other hand, Moradi et al. (2022), and Kohantorabi et al. (2021) suggested that apart from the Fe ions, the photogenerated e^- can also activate PS and PMS, respectively, to generate $SO_4^{\bullet-}$ radicals. Thereby, Moradi et al. (2022) explained that PS activation to produce $SO_4^{\bullet-}$ can be fulfilled by the Fe and Co ions of SCF, the photogenerated e^- in the conduction band of g-C_3N_4, or the photolysis of PS via UV light. Additionally, Kohantorabi et al. (2021) determined that the photogenerated e^- as well as Fe^{2+}/Fe^{3+} and Ce^{4+}/Ce^{3+} redox cycles can also be involved in the PMS activation. In view of the studies of Grzegórska et al. (2023), Moradi et al. (2022) and Kohantorabi et al. (2021), it may be considered that the magnetic component of the photocatalyst can also be an activator of PS/PMS through the ions (e.g., Fe ions) that constitute it. Additionally, it is worth mentioning that both Fe_3O_4 and ferrites have been employed for preparing photocatalysts to degrade contaminants via PMS/PS-based AOPs. However, as seen in Table 5, ferrites have been predominantly used in most of the works that exploit this function of the photocatalyst's magnetic component. This preference may be attributed to the attractive features of ferrites coupled with the presence of ions (including, Fe, Mn, Co) that could act as PS/PMS activators (Moradi et al., 2022; Grzegórska et al., 2023; Tian et al., 2023; Zheng et al., 2024). In this regard, Song et al. (2024) found that the ferrite $CuFe_2O_4$ yielded degradation efficiencies exceeding 65% for the three contaminants they investigated (tetracycline, 2-nitrophenol, ceftriaxone sodium) within the $CuFe_2O_4$/PMS/Vis system, which demonstrates that $CuFe_2O_4$ alone exhibits high effectiveness in the degradation of pollutants. Similarly, Hao et al. (2024) reported 70% tetracycline removal by the MOF-derived $CoFe_2O_4$/PS/Vis system, which also substantiates the ability of MOF-derived $CoFe_2O_4$ for degrading pollutants. In contrast to what is reported in these works, Feng et al. (2023) found that $BaFe_{12}O_{19}$ hardly degrades tetracycline (16.3%) over the $BaFe_{12}O_{19}$/PMS/Vis system; they explained that $BaFe_{12}O_{19}$ weakly activates PMS due to the fast recombination of the

photogenerated charges in the ferrite. On the other hand, it can be also noted from Table 5 that visible light has been used in most of the studies for promoting pollutant removal. Additionally, UVC and UVA light irradiation have been employed to assist the degradation process.

Collectively, the incorporation of magnetic materials to the photocatalyst not only benefits the retrieval of the composite from the treated medium but could also enhance the photocatalytic degradation of contaminants. Specifically, the magnetic materials can play different roles, namely, active catalyst, PS/PMS activator, conduction medium and activation of Fenton-like oxidation, apart from assisting the magnetic recovery of the photocatalyst as it has been discussed throughout this section. It is worth mentioning that the magnetic constituent can exclusively act as photocatalyst, as proposed, for instance in the works of Huang et al. (2023), Jiang X. et al. (2022), Wang et al. (2021), and Karbasi et al. (2019). Alternatively, it can combine this function with its role as PMS activator or component of the Fenton-like oxidation as suggested by Tian et al. (2023), Moradi et al. (2022), and Banic et al. (2019), to name a few.

3 Design of magnetic separators for photocatalyst recovery

Throughout the previous sections the attractive prospects of using magnetic photocatalysts for degrading organic pollutants have been comprehensively outlined. It is noteworthy that although integrating semiconductors and magnetic components could enhance the photocatalytic performance, the primary focus of compositing these materials lies in facilitating their recovery after use. Nevertheless, from the numerous works surveyed herein, only a limiting few have assessed the ability of magnetic photocatalysts for being magnetically recovered. This preliminary test is typically based on placing a permanent magnet next to a vial containing a sample of the suspended magnetic photocatalysts; after a certain time period, a clear solution, with the particles retained in the vial wall close to the magnet is obtained (Fung et al., 2019; Wang et al., 2021; Grzegórska et al., 2023). While this methodology enables ascertaining whether the photocatalyst can be magnetically retrieved, the time required for recovering the magnetic photocatalyst from the entire volume of the medium, which is crucial for determining the efficiency of the magnetic recovery stage, is not estimated. On a similar note, the design of magnetic separators for addressing the recovery of magnetic photocatalysts remains an area that has received limited attention. Particularly, only Kumar et al. (2019) and Fernández et al. (2019) have addressed both the recovery of the composites from the total volume of the medium and the use of a specific magnetic separation system to perform such retrieval. Specifically, Kumar et al. (2019) employed an electromagnetic separation unit, where the retrieval of the composites due to the action of the applied electromagnetic field (~200 mT) was accomplished. Additionally, they also determined the efficiency of the electromagnetic separation unit for retrieving the composite as a function of time by measuring the turbidity of supernatant samples taken at different times. Fernández et al. (2019) utilized a magnetic photocatalytic reactor to carry out the photodegradation of the pollutants followed by the magnetic retrieval of the photocatalysts. The magnetic separation unit features an alternate polarity magnetic bar, where the magnetic photocatalyst was trapped after use. Thereby, the research conducted by Kumar et al. (2019) and Fernández et al. (2019) provide a more realistic picture about the use of magnetic photocatalysts by integrating the photocatalytic degradation step and the subsequent magnetic recovery.

Although magnetic separators have not been typically used in the studies covered by the present work, the efficiency of several systems for retrieving magnetic materials has been evidenced in existing literature. For instance, high gradient magnetic separators (HGMSs) have been applied in several fields for the separation of magnetic solids, including wastewater treatment (Baik et al., 2012; Gómez-Pastora et al., 2017a, Gómez-Pastora et al., 2017b; Kheshti et al., 2019). Briefly, HGMSs comprise batch filters filled with ferromagnetic filaments (Figure 4A) and can use different sources for generating the magnetic field. When an external magnetic field is applied, these filters trap the magnetic materials, thus obtaining a clean solution; subsequently, the magnetic materials can be recovered from the HGMSs by switching off the magnetic field. Despite the high efficiency provided by HGMSs, they pose several drawbacks, such as the undesired entrapment of non-magnetic solids or the possible particle aggregation, which could limit their practical application (Leong et al., 2016; Gómez-Pastora et al., 2017b). Another alternative for addressing the retrieval of magnetic materials consists of the use of open gradient magnetic separators (OGMSs), which are not based on ferromagnetic matrices. In OGMSs, magnetic fields are generated by magnets conveniently arranged around the separator walls. OGMSs provide high separation efficacy; however, their lower magnetic gradients compared to HGMSs represent an important drawback. In this regard, magnetic gradients may be considerably increased by using powerful magnets in quadrupole configuration, which is one of the most common magnet arrangements. Particularly, in the continuous OGMSs with the quadrupole magnet configuration, magnetic materials and the clean solution are obtained at different outlets of the system under a magnetic field as shown in Figure 4B (Gómez-Pastora et al., 2017a; Gómez-Pastora et al., 2017b).

The design of magnetic separators requires understanding the physics underlying photocatalysts retrieval. Particularly, magnetic separation is driven by the magnetic force exerted on magnetic photocatalysts (F_m), which is described by the following expression (Furlani, 2006; Furlani, 2010):

$$\mathbf{F_m} = \boldsymbol{\mu_0} \mathbf{V_p} (\mathbf{Mp} \cdot \nabla) \mathbf{H_a} \tag{12}$$

where, μ_0 denotes the permeability of free space, V_p and Mp stand for the particle volume and magnetization, and H_a represents the applied magnetic field intensity (Furlani, 2006, Furlani, 2010).

According to the Eq. 12, F_m is proportional to the volume and saturation magnetization of the photocatalytic particle. Hence, magnetic recovery is favored for large particles. However, increasing the particle size causes the reduction of its surface to volume ratio, thus negatively affecting the efficacy of the photocatalyst. On the other hand, the higher the particle

saturation magnetization the greater the F_m that promotes its retrieval from the treated solution. Nevertheless, the saturation magnetization decreases when the magnetic constituent is compound with semiconductors, as it has been previously discussed (Gómez-Pastora et al., 2017b; Torrejon et al., 2020). In this context, it becomes evident that a trade-off between the factors influencing photocatalytic degradation and magnetic separation should be achieved so that both of them could be optimized. Additionally, desired magnetic separators will ensure complete retrieval of photocatalyst while providing high-volumetric throughput. To design systems that fulfill these requirements, simulation software could be employed, since they can provide insight into the magnetic and hydrodynamic conditions in the separators (Figure 4C). In this regard, computational fluid dynamics (CFD) techniques enable modeling the separation process prior to the system fabrication, and their potential for contributing to the design of magnetic separators have been already demonstrated. While CFD offers numerous benefits, it is important to recognize that the computational demand of the simulations could limit the complexity of the separators to be simulated (Gómez-Pastora et al., 2017b; González Fernández et al., 2020; González-Fernández et al., 2021).

4 Further directions and concluding remarks

Magnetic photocatalysts have gained recognition as potential agents to assist the photodegradation of organic pollutants. Thereby, the integration of semiconductors with magnetic materials enables surmounting a critical challenge in photocatalysis, namely the post-use recovery of the photocatalyst. Additionally, magnetic photocatalysts have been acknowledged for their possibilities to enhance the photocatalytic performance through different functions. However, despite the promising prospects of magnetic photocatalysts, there are still open questions that need to be addressed so that these composites could be applied in large scale water treatment process. These issues pertain to the two main steps of photocatalytic processes, which include the efficient degradation of target pollutants and the subsequent retrieval of the photocatalyst.

Regarding the pollutants removal step, it is crucial to enhance to a great extent the photocatalyst's performance so that the complete degradation of the target contaminants is efficiently accomplished. In this context, thorough research is essential to confirm and provide evidence for the possible functions of the photocatalyst's magnetic constituents, since these photocatalytic roles derive from the photocatalytic mechanism proposed in the surveyed studies. Additionally, to deepen the understanding of how magnetic materials contribute to enhance photodegradation, it is necessary to evaluate the photocatalyst's effectiveness both with and without the magnetic components, and compare the performance of photocatalysts comprising comparable concentrations of magnetic constituents. The absence of such comparative analysis in many studies listed in Tables 1–5 limits elucidating the impact of the magnetic component. The aforementioned insights could have the potential to significantly improve the photodegradation of pollutants by exploiting the photocatalytic roles of the magnetic components. In addition to better understanding the role of the magnetic component in photocatalysis, improving photocatalytic efficiency also requires assessing photocatalytic performance under conditions that closely resemble real environmental scenarios. In this regard, the lack of correlation of the photocatalysts efficiency in well-controlled lab conditions and in real-world applications has been reported to greatly contribute to the scarce use of photocatalysis in the latter (Bortolotto et al., 2022). Exploring the photocatalyst's efficiency in a medium constituted of a mixture of pollutants, rather than a single one could contribute to bridge the gap between the experimental and real-world conditions encountered in photocatalysis. Finally, advancing in the design of magnetic photocatalysts also requires assessing their performance for pollutant mineralization and monitoring the potential metal leaching during their use. Leaching measurements in several studies revealed a release of metal ions typically lower than 4.6 mg/L, suggesting that there are no significant safety hazards to the aquatic environment. However, total organic carbon (TOC) analysis showed that target contaminants were not fully mineralized into CO_2, but TOC yield of removal lower than 70% are normally obtained. Despite the importance of conducting leaching and TOC analyses, they have only been carried out in some works included in Tables 1–5. Hence, future research should incorporate these analyses to enhance the performance of novel magnetic photocatalysts.

Regarding the magnetic retrieval of the photocatalysts, the practical use of magnetic photocatalysts also requires the implementation of the magnetic separation stage, as well as its integration with the previous photocatalytic process. From this perspective, it is vitally important to demonstrate efficient recovery of magnetic photocatalysts that extends beyond the small-scale proof-of-concept assays reported in most studies. Hence, research efforts should be devoted to the design and optimization of magnetic separators for addressing the efficient recovery of the magnetic photocatalysts after use. More specifically, there is an urgent need for developing magnetic separators that ensure complete photocatalyst retrieval while providing high-volume throughput. CFD techniques can guide the enhancement of the systems performance through the strategic refinement of different features, including the separator geometry or the applied magnetic fields and gradients (Gómez-Pastora et al., 2017b; González Fernández et al., 2020; González-Fernández et al., 2021).

Overall, this study offers a comprehensive overview of the potential of magnetic photocatalysts for the oxidation of organic pollutants from aquatic environments. Particularly, we have reviewed articles that cover the last 6 years of research to underscore the dual role of magnetic photocatalysts. Thereby, in addition to emphasizing the ease retrieval of magnetic photocatalysts by applying magnetic fields, a challenge that has received considerable attention, this study also focuses on the less examined photocatalytic roles of the photocatalyst's magnetic constituents. Additionally, we have highlighted the importance of further research to advance the use of magnetic photocatalysts as outstanding materials in real applications. Collectively, this review envisages great hopes for the exploitation of the magnetically assisted photocatalysis for degradation of organic pollutants, which may stimulate further progress on this field and its exploitation for a broader range of photocatalytic processes beyond the removal of contaminants.

Author contributions

CG-F: Conceptualization, Formal Analysis, Investigation, Writing–original draft. EB: Funding acquisition, Methodology, Visualization, Writing–review and editing. MR: Conceptualization, Funding acquisition, Supervision, Writing–review and editing. IO: Funding acquisition, Project administration, Resources, Supervision, Writing–review and editing.

Funding

The author(s) declare that financial support was received for the research, authorship, and/or publication of this article. Financial support from the project PID2021-122563OB-I00 funded by MICIU/AEI/10.13039/501100011033 and by ERDF/EU and Grant PLEC2021-007718 funded by MICIU/AEI/10.13039/501100011033 and by the European Union NextGenerationEU/PRTR are gratefully acknowledged. CG-F also thanks the Spanish Ministry of Universities for the Margarita Salas postdoctoral fellowship (grants for the requalification of the Spanish university system for 2021–2023, University of Cantabria), funded by the European Union-NextGenerationEU.

Conflict of interest

The authors declare that the research was conducted in the absence of any commercial or financial relationships that could be construed as a potential conflict of interest.

Publisher's note

References

Abdel-Wahed, M. S., El-Kalliny, A. S., Badawy, M. I., Attia, M. S., and Gad-Allah, T. A. (2020). Core double-shell $MnFe_2O_4$@rGO@TiO_2 superparamagnetic photocatalyst for wastewater treatment under solar light. *Chem. Eng. J.* 382, 122936. doi:10.1016/j.cej.2019.122936

Adeola, A. O., Abiodun, B. A., Adenuga, D. O., and Nomngongo, P. N. (2022). Adsorptive and photocatalytic remediation of hazardous organic chemical pollutants in aqueous medium: a review. *J. Contam. Hydrol.* 248, 104019. doi:10.1016/j.jconhyd.2022.104019

Ahmadpour, N., Sayadi, M. H., Sobhani, S., and Hajiani, M. (2020). Photocatalytic degradation of model pharmaceutical pollutant by novel magnetic TiO_2@$ZnFe_2O_4$/Pd nanocomposite with enhanced photocatalytic activity and stability under solar light irradiation. *J. Environ. Manage.* 271, 110964. doi:10.1016/j.jenvman.2020.110964

Alvarez-Aguiñaga, E. A., Elizalde-González, M. P., García-Díaz, E., and Sabinas-Hernández, S. A. (2022). UV-light-driven conversion of gadoterate meglumine: insight into the photocatalyst's influence on conversion pathway, transformation products, and release of toxic ionic gadolinium. *Catal. Commun.* 172, 106544. doi:10.1016/j.catcom.2022.106544

Arman, N. Z., Salmiati, S., Aris, A., Salim, M. R., Nazifa, T. H., Muhamad, M. S., et al. (2021). A review on emerging pollutants in the water environment: existences, health effects and treatment processes. *Water* 13, 3258. doi:10.3390/w13223258

Bahmani, M., Dashtian, K., Mowla, D., Esmaeilzadeh, F., and Ghaedi, M. (2020). UiO-66(Ti)-Fe_3O_4-WO_3 photocatalyst for efficient ammonia degradation from wastewater into continuous flow-loop thin film slurry flat-plate photoreactor. *J. Hazard. Mater.* 393, 122360. doi:10.1016/j.jhazmat.2020.122360

Baik, S. K., Ha, D. W., Ko, R. K., and Kwon, J. M. (2012). Magnetic field analysis of high gradient magnetic separator via finite element analysis. *Phys. C Supercond. its Appl.* 480, 111–117. doi:10.1016/j.physc.2012.04.036

Banic, N. D., Abramovic, B. F., Krstic, J. B., Šojiic Merkulova, D. V., Fincur, N. L., and Mitric, M. N. (2019). Novel WO_3/Fe_3O_4 magnetic photocatalysts: preparation, characterization and thiacloprid photodegradation. *J. Ind. Eng. Chem.* 70, 264–275. doi:10.1016/j.jiec.2018.10.025

Behnajady, M. A., Hajiahmadi, M., and Modirshahla, N. (2012). Enhancement of removal rate of an organic pollutant in the presence of immobilized TiO_2 nanoparticles with inorganic anions combination: optimization using Taguchi approach. *Ind. Eng. Chem. Res.* 51, 15324–15330. doi:10.1021/ie301521z

Belessiotis, G. V., Falara, P. P., Ibrahim, I., and Kontos, A. G. (2022). Magnetic metal oxide-based photocatalysts with integrated silver for water treatment. *Materials* 15, 4629. doi:10.3390/ma15134629

Bhatkhande, D. S., Pangarkar, V. G., and Beenackers, A. A. C. M. (2002). Photocatalytic degradation for environmental applications - a review. *J. Chem. Technol. Biotechnol.* 77, 102–116. doi:10.1002/jctb.532

Bielan, Z., Kowalska, E., Dudziak, S., Wang, K., Ohtani, B., and Zielińska-Jurek, A. (2021). Mono- and bimetallic (Pt/Cu) titanium(IV) oxide core–shell photocatalysts with UV/Vis light activity and magnetic separability. *Catal. Today* 361, 198–209. doi:10.1016/j.cattod.2020.05.034

Bielan, Z., Sulowska, A., Dudziak, S., Siuzdak, K., Ryl, J., and Zielińska-Jurek, A. (2020). Defective TiO_2 core-shell magnetic photocatalyst modified with plasmonic nanoparticles for visible light-induced photocatalytic activity. *Catalysts* 10, 672. doi:10.3390/catal10060672

Bortolotto, V., Djellabi, R., Giordana, A., Cerrato, G., Di Michele, A., and Bianchi, C. L. (2022). Photocatalytic behaviour of Ag_3PO_4, Fe_3O_4 and Ag_3PO_4/Fe_3O_4 heterojunction towards the removal of organic pollutants and Cr (VI) from water: efficiency and light-corrosion deactivation. *Inorg. Chem. Commun.* 141, 109516. doi:10.1016/j.inoche.2022.109516

Bule Možar, K., Miloloža, M., Martinjak, V., Radovanović-Perić, F., Bafti, A., Ujević Bošnjak, M., et al. (2024). Evaluation of Fenton, photo-fenton and fenton-like processes in degradation of PE, PP, and PVC microplastics. *WaterSwitzerl.* 16, 673. doi:10.3390/w16050673

Casbeer, E., Sharma, V. K., and Li, X. Z. (2012). Synthesis and photocatalytic activity of ferrites under visible light: a review. *Sep. Purif. Technol.* 87, 1–14. doi:10.1016/j.seppur.2011.11.034

Chávez, A. M., Quiñones, D. H., Rey, A., Beltrán, F. J., and Álvarez, P. M. (2020). Simulated solar photocatalytic ozonation of contaminants of emerging concern and effluent organic matter in secondary effluents by a reusable magnetic catalyst. *Chem. Eng. J.* 398, 125642. doi:10.1016/j.cej.2020.125642

Chen, Z., Yan, Y., Lu, C., Lin, X., Fu, Z., Shi, W., et al. (2023). Photocatalytic self-fenton system of g-C_3N_4-based for degradation of emerging contaminants: a review of advances and prospects. *Molecules* 28, 5916. doi:10.3390/molecules28155916

Chen, Z. Y., Lai, W. W. P., Lin, H. H. H., Tan, J. X., Wu, K. C. W., and Lin, A. Y. C. (2022). Photocatalytic degradation of ketamine using a reusable TiO_2/SiO_2@Fe_3O_4 magnetic photocatalyst under simulated solar light. *J. Environ. Chem. Eng.* 10, 108637. doi:10.1016/j.jece.2022.108637

Cheng, N., Wang, B., Wu, P., Lee, X., Xing, Y., Chen, M., et al. (2021). Adsorption of emerging contaminants from water and wastewater by modified biochar: a review. *Environ. Pollut.* 273, 116448. doi:10.1016/j.envpol.2021.116448

Cheng, Y., Zhang, S., Wang, Z., Wang, B., You, J., Guo, R., et al. (2023). Review on spinel ferrites-based materials (MFe_2O_4) as photo-Fenton catalysts for degradation of organic pollutants. *Sep. Purif. Technol.* 318, 123971. doi:10.1016/j.seppur.2023.123971

Dewil, R., Mantzavinos, D., Poulios, I., and Rodrigo, M. A. (2017). New perspectives for advanced oxidation processes. *J. Environ. Manage.* 195, 93–99. doi:10.1016/j.jenvman.2017.04.010

Dharma, H. N. C., Jaafar, J., Widiastuti, N., Matsuyama, H., Rajabsadeh, S., Othman, M. H. D., et al. (2022). A review of titanium dioxide (TiO_2)-based photocatalyst for oilfield-produced water treatment. *Membranes* 12, 345. doi:10.3390/membranes12030345

do Carmo Batista, W. V. F., da Cunha, R., dos Santos, A. C., dos Reis, P. M., Furtado, C. A., Silva, M. C., et al. (2022). Synthesis of a reusable magnetic photocatalyst based on carbon xerogel/TiO_2 composites and its application on acetaminophen degradation. *Ceram. Int.* 48, 34395–34404. doi:10.1016/j.ceramint.2022.08.018

Dudziak, S., Bielan, Z., Kubica, P., and Zielinska-Jurek, A. (2021). Optimization of carbamazepine photodegradation on defective TiO_2-based magnetic photocatalyst. *J. Environ. Chem. Eng.* 9, 105782. doi:10.1016/j.jece.2021.105782

Feng, S., Xie, T., Wang, J., Yang, J., Kong, D., Liu, C., et al. (2023). Photocatalytic activation of PMS over magnetic heterojunction photocatalyst $SrTiO_3/BaFe_{12}O_{19}$ for tetracycline ultrafast degradation. *Chem. Eng. J.* 470, 143900. doi:10.1016/j.cej.2023.143900

Fernández, L., Gamallo, M., González-Gómez, M. A., Vázquez-Vázquez, C., Rivas, J., Pintado, M., et al. (2019). Insight into antibiotics removal: exploring the photocatalytic performance of a Fe_3O_4/ZnO nanocomposite in a novel magnetic sequential batch reactor. *J. Environ. Manage.* 237, 595–608. doi:10.1016/j.jenvman.2019.02.089

Fung, C. S. L., Khan, M., Kumar, A., and Lo, I. M. C. (2019). Visible-light-driven photocatalytic removal of PPCPs using magnetically separable bismuth oxybromo-iodide solid solutions: mechanisms, pathways, and reusability in real sewage. *Sep. Purif. Technol.* 216, 102–114. doi:10.1016/j.seppur.2019.01.077

Furlani, E. P. (2006). Analysis of particle transport in a magnetophoretic microsystem. *J. Appl. Phys.* 99. doi:10.1063/1.2164531

Furlani, E. P. (2010). Magnetic biotransport: analysis and applications. *Materials* 3, 2412–2446. doi:10.3390/ma3042412

Fuziki, M. E. K., Brackmann, R., Dias, D. T., Tusset, A. M., Specchia, S., and Lenzi, G. G. (2021). Effects of synthesis parameters on the properties and photocatalytic activity of the magnetic catalyst $TiO_2/CoFe_2O_4$ applied to selenium photoreduction. *J. Water Process Eng.* 42, 102163. doi:10.1016/j.jwpe.2021.102163

Ganiyu, S. O., Nidheesh, P. V., and Oturan, M. A. (2022). "Synthesis and application of nanostructured iron oxides heterogeneous catalysts for environmental applications," in *Advanced materials for sustainable environmental remediation: terrestrial and aquatic environments*, 583–608.

Ghobadifard, M., Mohebbi, S., and Radovanovic, P. V. (2020). Selective oxidation of alcohols by using $CoFe_2O_4/Ag_2MoO_4$ as a visible-light-driven heterogeneous photocatalyst. *New J. Chem.* 44, 2858–2867. doi:10.1039/c9nj05633e

Gómez-Pastora, J., Dominguez, S., Bringas, E., Rivero, M. J., Ortiz, I., and Dionysiou, D. D. (2017a). Review and perspectives on the use of magnetic nanophotocatalysts (MNPCs) in water treatment. *Chem. Eng. J.* 310, 407–427. doi:10.1016/j.cej.2016.04.140

Gómez-Pastora, J., Xue, X., Karampelas, I. H., Bringas, E., Furlani, E. P., and Ortiz, I. (2017b). Analysis of separators for magnetic beads recovery: from large systems to multifunctional microdevices. *Sep. Purif. Technol.* 172, 16–31. doi:10.1016/j.seppur.2016.07.050

González Fernández, C., Gómez Pastora, J., Basauri, A., Fallanza, M., Bringas, E., Chalmers, J. J., et al. (2020). Continuous-flow separation of magnetic particles from biofluids: how does the microdevice geometry determine the separation performance? *Sensors* 20, 3030. doi:10.3390/s20113030

González-Fernández, C., Gómez-Pastora, J., Bringas, E., Zborowski, M., Chalmers, J. J., and Ortiz, I. (2021). Recovery of magnetic catalysts: advanced design for process intensification. *Ind. Eng. Chem. Res.* 60, 16780–16790. doi:10.1021/acs.iecr.1c03474

González-Rodríguez, J., Conde, J. J., Vargas-Osorio, Z., Vázquez-Vázquez, C., Piñeiro, Y., Rivas, J., et al. (2024). LED-driven photo-Fenton process for micropollutant removal by nanostructured magnetite anchored in mesoporous silica. *J. Environ. Manage.* 349, 119461. doi:10.1016/j.jenvman.2023.119461

Grzegórska, A., Ofoegbu, J. C., Cervera-Gabalda, L., Gómez-Polo, C., Sannino, D., and Zielińska-Jurek, A. (2023). Magnetically recyclable TiO_2/MXene/$MnFe_2O_4$ photocatalyst for enhanced peroxymonosulphate-assisted photocatalytic degradation of carbamazepine and ibuprofen under simulated solar light. *J. Environ. Chem. Eng.* 11, 110660. doi:10.1016/j.jece.2023.110660

Guo, R., Xi, B., Guo, C., Liu, W., Lv, N., and Xu, J. (2022). Comprehensive insight into heterogeneous persulfate activation for environmental pollutants degradation: approaches and mechanism. *Environ. Funct. Mater.* 1, 239–252. doi:10.1016/j.efmat.2022.12.001

Gupta, N. K., Ghaffari, Y., Kim, S., Bae, J., Kim, K. S., and Saifuddin, M. (2020). Photocatalytic degradation of organic pollutants over MFe_2O_4 (M = Co, Ni, Cu, Zn) nanoparticles at neutral pH. *Sci. Rep.* 10, 4942. doi:10.1038/s41598-020-61930-2

Han, Y., Wang, S., Yu, X., Li, M., Yi, Z., Tang, J., et al. (2023). $Ba_{0.5}Sr_{0.5}TiO_3/BaFe_{12}O_{19}$ magnetic separation photocatalysts: structural, optical, microstructure, photocatalytic activity, degradation pathway and mechanism. *Ceram. Int.* 49, 37967–37982. doi:10.1016/j.ceramint.2023.09.126

Hao, Y., Yang, H., Jiang, S., Komarneni, S., and Ma, J. (2024). MOF-derived $CoFe_2O_4/FeS_2$ Z-type heterojunctions for efficient degradation of tetracycline by visible-light activation of persulfate. *Ceram. Int.* 50, 25365–25378. doi:10.1016/j.ceramint.2024.04.268

He, J., Zeng, X., Lan, S., and Lo, I. M. C. (2019). Reusable magnetic Ag/Fe, N-TiO_2/Fe_3O_4@SiO_2 composite for simultaneous photocatalytic disinfection of E. coli and degradation of bisphenol A in sewage under visible light. *Chemosphere* 217, 869–878. doi:10.1016/j.chemosphere.2018.11.072

Huang, H., Tao, X., Niu, Z., Qin, X., Ren, J., Shan, B., et al. (2023). Construction of magnetically recoverable $MnZnFe_2O_4$@Ag_3PO_4 Z-scheme photocatalyst for rapid visible-light-driven phenol degradation. *Environ. Sci. Pollut. Res.* 30, 32095–32107. doi:10.1007/s11356-022-24479-3

Iglesias, O., Rivero, M. J., Urtiaga, A. M., and Ortiz, I. (2016). Membrane-based photocatalytic systems for process intensification. *Chem. Eng. J.* 305, 136–148. doi:10.1016/j.cej.2016.01.047

Jabbar, Z. H., Graimed, B. H., Alsunbuli, M. M., and Sabit, D. A. (2023). Developing a magnetic bismuth-based quaternary semiconductor boosted by plasmonic action for photocatalytic detoxification of Cr(VI) and norfloxacin antibiotic under simulated solar irradiation: synergistic work and radical mechanism. *J. Alloys Compd.* 958, 170521. doi:10.1016/j.jallcom.2023.170521

Jiang, X., Wang, M., Luo, B., Yang, Z., Li, W., Zhang, D., et al. (2022). Magnetically recoverable flower-like $Sn_3O_4/SnFe_2O_4$ as a type-II heterojunction photocatalyst for efficient degradation of ciprofloxacin. *J. Alloys Compd.* 926, 166878. doi:10.1016/j.jallcom.2022.166878

Jiang, Y., Ran, J., Mao, K., Yang, X., Zhong, L., Yang, C., et al. (2022). Recent progress in Fenton/Fenton-like reactions for the removal of antibiotics in aqueous environments. *Ecotoxicol. Environ. Saf.* 236, 113464. doi:10.1016/j.ecoenv.2022.113464

Jung, Y. S., Lim, W. T., Park, J. Y., and Kim, Y. H. (2009). Effect of pH on Fenton and fenton-like oxidation. *Environ. Technol.* 30, 183–190. doi:10.1080/09593330802468848

Kamali, M., Xue, Y., Khalaj, M., Laats, B., Teunckens, R., Verbist, M., et al. (2022). ZnO/γ-Fe_2O_3/Bentonite: an efficient solar-light active magnetic photocatalyst for the degradation of pharmaceutical active compounds. *Molecules* 27, 3050. doi:10.3390/molecules27103050

Karbasi, M., Karimzadeh, F., Kiwi, J., Raeissi, K., Pulgarin, C., and Rtimi, S. (2019). Flower-like magnetized photocatalysts accelerating an emerging pollutant removal under indoor visible light and related phenomena. *J. Photochem. Photobiol. A Chem.* 378, 105–113. doi:10.1016/j.jphotochem.2019.04.017

Kefeni, K. K., and Mamba, B. B. (2020). Photocatalytic application of spinel ferrite nanoparticles and nanocomposites in wastewater treatment: review. *Sustain. Mater. Technol.* 23, e00140. doi:10.1016/j.susmat.2019.e00140

Khan, M., Fung, C. S. L., Kumar, A., He, J., and Lo, I. M. C. (2019a). Unravelling mechanistic reasons for differences in performance of different Ti- and Bi-based magnetic photocatalysts in photocatalytic degradation of PPCPs. *Sci. Total Environ.* 686, 878–887. doi:10.1016/j.scitotenv.2019.05.340

Khan, M., Fung, C. S. L., Kumar, A., and Lo, I. M. C. (2019b). Magnetically separable BiOBr/Fe_3O_4@SiO_2 for visible-light-driven photocatalytic degradation of ibuprofen: mechanistic investigation and prototype development. *J. Hazard. Mater.* 365, 733–743. doi:10.1016/j.jhazmat.2018.11.053

Kheshti, Z., Hassanajili, S., and Ghajar, K. A. (2019). Study and optimization of a high-gradient magnetic separator using flat and lattice plates. *IEEE Trans. Magn.* 55, 1–8. doi:10.1109/tmag.2018.2883624

Khosravani Goshtasb, Z., Mehdi Sabzehmeidani, M., Ghaedi, M., Madadi Avargani, V., and Moradi, Z. (2022). Magnetic Ag_3PO_4/Ag_2CrO_4/Fe/Fe_3O_4 quaternary composite for improved solar-driven photocatalytic degradation of cationic dyes under natural solar radiation. *J. Photochem. Photobiol. A Chem.* 428, 113856. doi:10.1016/j.jphotochem.2022.113856

Kisała, J., Vasile, B. S., Ficai, A., Ficai, D., Wojnarowska-Nowak, R., and Szreder, T. (2023). Reductive photodegradation of 4,4′-Isopropylidenebis(2,6-dibromophenol) on Fe_3O_4 surface. *Materials* 16, 4380. doi:10.3390/ma16124380

Klu, P. K., Nasir Khan, M. A., Wang, C., Qi, J., Sun, X., and Li, J. (2022). Mechanism of peroxymonosulfate activation and the utilization efficiency using hollow $(Co, Mn)_3O_4$ nanoreactor as an efficient catalyst for degradation of organic pollutants. *Environ. Res.* 207, 112148. doi:10.1016/j.envres.2021.112148

Kohantorabi, M., Moussavi, G., Oulego, P., and Giannakis, S. (2021). Radical-based degradation of sulfamethoxazole via UVA/PMS-assisted photocatalysis, driven by magnetically separable Fe_3O_4@CeO_2@BiOI nanospheres. *Sep. Purif. Technol.* 267, 118665. doi:10.1016/j.seppur.2021.118665

Kumar, A., Khan, M., Fang, L., and Lo, I. M. C. (2019). Visible-light-driven N-TiO 2 @SiO 2 @Fe 3 O 4 magnetic nanophotocatalysts: synthesis, characterization, and photocatalytic degradation of PPCPs. *J. Hazard. Mater.* 370, 108–116. doi:10.1016/j.jhazmat.2017.07.048

Kumar, U., Kuntail, J., Kumar, A., Prakash, R., Pai, M. R., and Sinha, I. (2022). *In-situ* H_2O_2 production for tetracycline degradation on Ag/s-(Co_3O_4/$NiFe_2O_4$) visible light magnetically recyclable photocatalyst. *Appl. Surf. Sci.* 589, 153013. doi:10.1016/j.apsusc.2022.153013

Kunarti, E. S., Roto, R., Sutarno, S., Budi, I. S., and Masdiansyah, M. (2021). Effective photocatalytic degradation of nitrobenzene by magnetite modified titania composite. *Asian J. Chem.* 33, 1319–1324. doi:10.14233/ajchem.2021.23137

Lendzion-Bielun, Z., Wojciechowska, A., Grzechulska-Damszel, J., Narkiewicz, U., Sniadecki, Z., and Idzikowski, B. (2020). Effective processes of phenol degradation on Fe3O4–TiO2 nanostructured magnetic photocatalyst. *J. Phys. Chem. Solids* 136, 109178. doi:10.1016/j.jpcs.2019.109178

Lenzi, G. G., Lopes, M. F., Andrade, D. I., Napoli, J. S., Parolin, A., Fávaro, Y. B., et al. (2021). Functioned catalysts with magnetic core applied in ibuprofen degradation. *Water Sci. Technol.* 84, 2158–2179. doi:10.2166/wst.2021.409

Leong, S. S., Yeap, S. P., and Lim, J. K. (2016). Working principle and application of magnetic separation for biomedical diagnostic at high- and low-field gradients. *Interface Focus* 6, 20160048. doi:10.1098/rsfs.2016.0048

Li, S., Wang, Z., Zhao, X., Yang, X., Liang, G., and Xie, X. (2019). Insight into enhanced carbamazepine photodegradation over biochar-based magnetic photocatalyst Fe_3O_4/BiOBr/BC under visible LED light irradiation. *Chem. Eng. J.* 360, 600–611. doi:10.1016/j.cej.2018.12.002

Li, Y., Zhai, Y., Zhang, P., Wang, X., Cui, H., Li, J., et al. (2019). Synthesis of titania coated magnetic activated carbon for effective photodegradation of tannic acid in aqueous solution. *Colloids Surfaces A Physicochem. Eng. Asp.* 563, 141–147. doi:10.1016/j.colsurfa.2018.11.025

Li, Z., Sun, Y., Liu, D., Yi, M., Chang, F., Li, H., et al. (2022). A review of sulfate radical-based and singlet oxygen-based advanced oxidation technologies: recent advances and prospects. *Catalysts* 12, 1092. doi:10.3390/catal12101092

Liu, M., Zhao, M., Tan, C., Ni, Y., Fu, Q., Li, H., et al. (2024). Effect of structural optimization of magnetic $MnFe_2O_4$@$Bi_{24}O_{31}Br_{10}$/Bi_5O_7I with core-shell structure on its enhanced photocatalytic activity to remove pharmaceuticals. *Colloids Surfaces A Physicochem. Eng. Asp.* 681, 132763. doi:10.1016/j.colsurfa.2023.132763

Liu, Z., Wang, G., Li, Y., Li, H., and Deng, N. (2024). Carboxymethyl-β-cyclodextrin functionalized TiO_2@Fe_3O_4@RGO magnetic photocatalyst for efficient photocatalytic degradation of tetracycline under visible light irradiation. *J. Environ. Chem. Eng.* 12, 113303. doi:10.1016/j.jece.2024.113303

Ma, H., and Liu, C. (2021). A mini-review of ferrites-based photocatalyst on application of hydrogen production. *Front. Energy* 15, 621–630. doi:10.1007/s11708-021-0761-0

Machado, F., Teixeira, A. C. S. C., and Ruotolo, L. A. M. (2023). Critical review of Fenton and photo-Fenton wastewater treatment processes over the last two decades. *Int. J. Environ. Sci. Technol.* 20, 13995–14032. doi:10.1007/s13762-023-05015-3

Mahato, M., Mukherjee, S., and Mishra, T. (2019). Development of magnetically separable mesoporous N doped TiO_2-SiO_2 coated Fe_3O_4 nanomaterial as solar photocatalyst for environmental application. *Mater. Res. Express* 6, 105544. doi:10.1088/2053-1591/ab432b

Mahmoudi, K., Farzadkia, M., Rezaei Kalantary, R., Sobhi, H. R., Yeganeh, M., and Esrafili, A. (2024). Efficient removal of oxytetracycline antibiotic from aqueous media using UV/g-C_3N_4/Fe_3O_4 photocatalytic process. *Heliyon* 10, e30604. doi:10.1016/j.heliyon.2024.e30604

Malinowska, I., Kubica, P., Madajski, P., Ostrowski, A., Gómez Polo, C., Carvera, L., et al. (2023). Synthesis, characterization, and application of 2D/2D TiO_2-GO-$ZnFe_2O_4$ obtained by the fluorine-free lyophilization method for solar light-driven photocatalytic degradation of ibuprofen. *Environ. Sci. Pollut. Res.* 30, 35929–35944. doi:10.1007/s11356-022-24587-0

Marghussian, V. (2015). "Magnetic properties of nano-glass ceramics," in *Nano-glass ceramics* (Elsevier), 181–223. doi:10.1016/b978-0-323-35386-1.00004-9

Moniriyan, F., Sabounchei, S. J., Yousefi, A., and Akhavan, O. (2021). Synthesis, morpho-structural properties, and catalytic performances of Pt-APA@Fe_3O_4/GO nanocomposite based on magnetical graphene in C–C coupling reactions and photoinactivation of E. coli. *J. Nanoparticle Res.* 23, 192. doi:10.1007/s11051-021-05278-2

Moradi, M., Kakavandi, B., Bahadoran, A., Giannakis, S., and Dehghanifard, E. (2022). Intensification of persulfate-mediated elimination of bisphenol A by a spinel cobalt ferrite-anchored g-C_3N_4 S-scheme photocatalyst: catalytic synergies and mechanistic interpretation. *Sep. Purif. Technol.* 285, 120313. doi:10.1016/j.seppur.2021.120313

Morin-Crini, N., Lichtfouse, E., Fourmentin, M., Ribeiro, A. R. L., Noutsopoulos, C., Mapelli, F., et al. (2022). Removal of emerging contaminants from wastewater using advanced treatments. A review. *Environ. Chem. Lett.* 20, 1333–1375. doi:10.1007/s10311-021-01379-5

Muhammad, W., Ali, W., Khan, M. A., Ali, F., Zada, A., Ansar, M. Z., et al. (2024). Construction of visible-light-driven 2D/2D $NiFe_2O_4$/g-C_3N_4 Z-scheme heterojunction photocatalyst for effective degradation of organic pollutants and CO_2 reduction. *J. Environ. Chem. Eng.* 12, 113409. doi:10.1016/j.jece.2024.113409

Niu, Z., Tao, X., Huang, H., Qin, X., Ren, C., Wang, Y., et al. (2022). Green synthesis of magnetically recyclable $Mn_{0.6}Zn_{0.4}Fe_2O_4$@$Zn_{1-x}Mn_xS$ composites from spent batteries for visible light photocatalytic degradation of phenol. *Chemosphere* 287, 132238. doi:10.1016/j.chemosphere.2021.132238

O'Dowd, K., and Pillai, S. C. (2020). Photo-Fenton disinfection at near neutral pH: process, parameter optimization and recent advances. *J. Environ. Chem. Eng.* 8, 104063. doi:10.1016/j.jece.2020.104063

Osanloo, M., Khorasheh, F., and Larimi, A. (2024). Fabrication of nano-dandelion magnetic TiO_2/$CuFe_2O_4$ doped with silver as a highly visible-light-responsive photocatalyst for degradation of Naproxen and Rhodamine B. *J. Mol. Liq.* 407, 125242. doi:10.1016/j.molliq.2024.125242

Oyekunle, D. T., Gendy, E. A., Ifthikar, J., and Chen, Z. (2022). Heterogeneous activation of persulfate by metal and non-metal catalyst for the degradation of sulfamethoxazole: a review. *Chem. Eng. J.* 437, 135277. doi:10.1016/j.cej.2022.135277

Preeyanghaa, M., Dhileepan, M. D., Madhavan, J., and Neppolian, B. (2022). Revealing the charge transfer mechanism in magnetically recyclable ternary g-C_3N_4/BiOBr/Fe_3O_4 nanocomposite for efficient photocatalytic degradation of tetracycline antibiotics. *Chemosphere* 303, 135070. doi:10.1016/j.chemosphere.2022.135070

Priyadarshini, M., Ahmad, A., Yadav, S., and Ghangrekar, M. M. (2024). Activation of persulphate by a waste-extracted metal–organic framework-derived iron oxide as a photocatalyst for effective degradation of salicylic acid. *J. Hazard. Toxic. Radioact. Waste* 28, 04024008. doi:10.1061/jhtrbp.hzeng-1308

Qi, C., Liu, X., Ma, J., Lin, C., Li, X., and Zhang, H. (2016). Activation of peroxymonosulfate by base: implications for the degradation of organic pollutants. *Chemosphere* 151, 280–288. doi:10.1016/j.chemosphere.2016.02.089

Radji, G., Bettahar, N., Bahmani, A., Boukhetache, I., and Contreras, S. (2022). Heterogeneous Fenton-like degradation of organic pollutants in petroleum refinery wastewater by copper-type layered double hydroxides. *J. Water Process Eng.* 50, 103305. doi:10.1016/j.jwpe.2022.103305

Rangaraj, V. M., Devaraju, S., Reddy, T. G., Zafar, H., Anjum, D. H., and Mittal, V. (2024). MOF-derived Co_3O_4@P-doped carbon nitride/α-Fe_2O_3 nanocomposite as a dual Z-scheme photocatalyst for persulfate mediated Bisphenol-A degradation. *Mater. Res. Bull.* 179, 112925. doi:10.1016/j.materresbull.2024.112925

Saif, H. M., Gebregeorgis, T. H., Crespo, J. G., and Pawlowski, S. (2024). The influence of flow electrode channel design on flow capacitive deionization performance: experimental and CFD modelling insights. *Desalination* 578, 117452. doi:10.1016/j.desal.2024.117452

Sangeetha, M., Ambika, S., Madhan, D., and Vadivel, S. (2024). Photocatalytic activity of Ag doped $CuFe_2O_4$ nanoparticles supported on reduced graphene oxide for the degradation of organic dyes under visible light irradiation. *J. Mater. Sci. Mater. Electron.* 35, 368. doi:10.1007/s10854-024-12076-8

Sayadi, M. H., Ahmadpour, N., and Homaeigohar, S. (2021). Photocatalytic and antibacterial properties of Ag-$CuFe_2O_4$@WO_3 magnetic nanocomposite. *Nanomaterials* 11, 298. doi:10.3390/nano11020298

Sepahvand, S., Bahrami, M., and Fallah, N. (2022). Photocatalytic degradation of 2,4-DNT in simulated wastewater by magnetic $CoFe_2O_4$/SiO_2/TiO_2 nanoparticles. *Environ. Sci. Pollut. Res.* 29, 6479–6490. doi:10.1007/s11356-021-13690-3

Shaheen, S., Xu, S., Bian, J., Zada, A., Zhang, Z. Q., Qu, Y., et al. (2024). Facile synthesis of hierarchical NiO/$NiFe_2O_4$ microsphere composite as efficient visible photocatalyst for 2,4-DCP degradation. *Rare Met.* 43, 1580–1588. doi:10.1007/s12598-023-02585-6

Sharma, S. K., Kumar, A., Sharma, G., Naushad, M., Ubaidullah, M., and García-Peñas, A. (2022). Developing a g-C_3N_4/$NiFe_2O_4$ S-scheme hetero-assembly for efficient photocatalytic degradation of cephalexin. *Colloids Surfaces A Physicochem. Eng. Asp.* 654, 129968. doi:10.1016/j.colsurfa.2022.129968

Singh, P., Sharma, K., Hasija, V., Sharma, V., Sharma, S., Raizada, P., et al. (2019). Systematic review on applicability of magnetic iron oxides–integrated photocatalysts for degradation of organic pollutants in water. *Mater. Today Chem.* 14, 100186. doi:10.1016/j.mtchem.2019.08.005

Smułek, W., Bielan, Z., Pacholak, A., Zdarta, A., Zgoła-Grześkowiak, A., Zielińska-Jurek, A., et al. (2021). Nitrofurazone removal from water enhanced by coupling photocatalysis and biodegradation. *Int. J. Mol. Sci.* 22, 2186. doi:10.3390/ijms22042186

Song, D., Zheng, Z., Wang, Z., Zhao, M., Ding, L., Zhang, Q., et al. (2024). Catalytic PMS oxidation universality of $CuFe_2O_4$/MnO_2 heterojunctions at multiple application scenarios. *Environ. Res.* 243, 117828. doi:10.1016/j.envres.2023.117828

Sonu, Dutta, V., Sharma, S., Raizada, P., Hosseini-Bandegharaei, A., Kumar Gupta, V., et al. (2019). Review on augmentation in photocatalytic activity of $CoFe_2O_4$ via heterojunction formation for photocatalysis of organic pollutants in water. *J. Saudi Chem. Soc.* 23, 1119–1136. doi:10.1016/j.jscs.2019.07.003

Sun, H., Wang, L., Wang, X., Dong, Y., and Pei, T. (2024). A magnetically recyclable Fe_3O_4/$ZnIn_2S_4$ type-II heterojunction to boost photocatalytic degradation of gemifloxacin. *Appl. Surf. Sci.* 656, 159674. doi:10.1016/j.apsusc.2024.159674

Surana, D., Gupta, J., Sharma, S., Kumar, S., and Ghosh, P. (2022). A review on advances in removal of endocrine disrupting compounds from aquatic matrices: future perspectives on utilization of agri-waste based adsorbents. *Sci. Total Environ.* 826, 154129. doi:10.1016/j.scitotenv.2022.154129

Tao, Y., Fan, G., Li, X., Cao, X., Du, B., Li, H., et al. (2024). Recyclable magnetic AgBr/BiOBr/Fe_3O_4 photocatalytic activation peroxymonosulfate for carbamazepine degradation: synergistic effect and mechanism. *Sep. Purif. Technol.* 330, 125392. doi:10.1016/j.seppur.2023.125392

Thomas, N., Dionysiou, D. D., and Pillai, S. C. (2021). Heterogeneous Fenton catalysts: a review of recent advances. *J. Hazard. Mater.* 404, 124082. doi:10.1016/j.jhazmat.2020.124082

Tian, N., Giannakis, S., Akbarzadeh, L., Hasanvandian, F., Dehghanifard, E., and Kakavandi, B. (2023). Improved catalytic performance of ZnO via coupling with $CoFe_2O_4$ and carbon nanotubes: a new, photocatalysis-mediated peroxymonosulfate activation system, applied towards Cefixime degradation. *J. Environ. Manage.* 329, 117022. doi:10.1016/j.jenvman.2022.117022

Torrejon, J., Raposo, V., Martinez, E., del Real, R. P., and Hayashi, M. (2020). *Current-induced dynamics of chiral domain walls in magnetic heterostructures*. 2nd Edn. Elsevier Ltd. doi:10.1016/B978-0-08-102832-2.00010-4

Tsaridou, C., and Karabelas, A. J. (2021). Drinking water standards and their implementation— a critical assessment. *WaterSwitzerl.* 13, 2918. doi:10.3390/w13202918

Vale, F., Sousa, C. A., Sousa, H., Santos, L., and Simões, M. (2022). Parabens as emerging contaminants: environmental persistence, current practices and treatment processes. *J. Clean. Prod.* 347, 131244. doi:10.1016/j.jclepro.2022.131244

Wang, H., Liu, H., Chu, Z., Sun, F., Zou, X., Wang, Q., et al. (2024a). Fe_3O_4 derived from the decomposition of siderite as a heterogeneous photocatalyst to degrade 2,4-dichlorophenol via activating PMS. *J. Water Process Eng.* 57, 104538. doi:10.1016/j.jwpe.2023.104538

Wang, R., Zhu, P., Liu, M., Xu, J., Duan, M., and Luo, D. (2021). Synthesis and characterization of magnetic $ZnFe_2O_4/Bi^0$-Bi_2MoO_6 with Z-scheme heterojunction for antibiotics degradation under visible light. *Sep. Purif. Technol.* 277, 119339. doi:10.1016/j.seppur.2021.119339

Wang, Y., Zhao, L., Cai, X., Chen, Y., Xu, J., Zhang, L., et al. (2024b). Construction of site-specific magnetic Z-scheme CdS/Fe_3O_4@N-doped graphene aerogel microtube/N-doped TiO_2 with porous structure: enhanced catalytic performance in photo-Fenton reaction. *Environ. Sci. Pollut. Res.* 31, 15091–15104. doi:10.1007/s11356-024-32190-8

Wu, Q., Siddique, M. S., Wang, H., Cui, L., Wang, H., Pan, M., et al. (2023). Visible-light-driven iron-based heterogeneous photo-Fenton catalysts for wastewater decontamination: a review of recent advances. *Chemosphere* 313, 137509. doi:10.1016/j.chemosphere.2022.137509

Wu, Q., and Song, Y. (2023). Recent advances in spinel ferrite-based magnetic photocatalysts for efficient degradation of organic pollutants. *Water Sci. Technol.* 87, 1465–1495. doi:10.2166/wst.2023.077

Wu, Y., Fang, Z., Shi, Y., Chen, H., Liu, Y., Wang, Y., et al. (2019). Activation of peroxymonosulfate by $BiOCl@Fe_3O_4$ catalyst for the degradation of atenolol: kinetics, parameters, products and mechanism. *Chemosphere* 216, 248–257. doi:10.1016/j.chemosphere.2018.10.012

Xie, L., Ren, Z., Zhu, P., Xu, J., Luo, D., and Lin, J. (2021). A novel CeO_2–TiO_2/PANI/$NiFe_2O_4$ magnetic photocatalyst: preparation, characterization and photodegradation of tetracycline hydrochloride under visible light. *J. Solid State Chem.* 300, 122208. doi:10.1016/j.jssc.2021.122208

Xu, G., Du, M., Li, T., Guan, Y., and Guo, C. (2021). Facile synthesis of magnetically retrievable $Fe_3O_4/BiVO_4$/CdS heterojunction composite for enhanced photocatalytic degradation of tetracycline under visible light. *Sep. Purif. Technol.* 275, 119157. doi:10.1016/j.seppur.2021.119157

Xue, Q., Song, B., Feng, Q., Yu, Z., Hu, K., Yang, Y., et al. (2024). Efficiently removal of tetracycline via synergistic photocatalysis with Fenton reaction with biochar/FeOOH. *Appl. Surf. Sci.* 645, 158869. doi:10.1016/j.apsusc.2023.158869

Yilmaz, M., Mengelizadeh, N., Saloot, M. K., Shahbaksh, S., and Balarak, D. (2022). Facile synthesis of Fe_3O_4/ZnO/GO photocatalysts for decolorization of acid blue 113 under solar, visible and UV lights. *Mater. Sci. Semicond. process.* 144, 106593. doi:10.1016/j.mssp.2022.106593

Younis, S. A., and Kim, K. H. (2020). Heterogeneous photocatalysis scalability for environmental remediation: opportunities and challenges. *Catalysts* 10, 1109. doi:10.3390/catal10101109

Yu, X., Sun, J., Li, G., Huang, Y., Li, Y., Xia, D., et al. (2020). Integration of $^{\bullet}SO4^{-}$-based AOP mediated by reusable iron particles and a sulfidogenic process to degrade and detoxify Orange II. *Water Res.* 174, 115622. doi:10.1016/j.watres.2020.115622

Zahedifar, M., and Seyedi, N. (2022). Bare 3D-TiO2/magnetic biochar dots (3D-TiO_2/BCDs MNPs): highly efficient recyclable photocatalyst for diazinon degradation under sunlight irradiation. *Phys. E Low-dimensional Syst. Nanostructures* 139, 115151. doi:10.1016/j.physe.2022.115151

Zhao, M., Wang, Y., Liu, M., Chen, W., Lin, Y., Li, C., et al. (2022). Photocatalytic treatment for antibacterials wastewater with high-concentration using $ZnFe_2O_4/Bi_7O_9I_3$ magnetic composite with optimized morphology and structure. *Colloids Surfaces A Physicochem. Eng. Asp.* 649, 129375. doi:10.1016/j.colsurfa.2022.129375

Zheng, Z., He, J., Zhang, Z., Kumar, A., Khan, M., Lung, C. W., et al. (2024). Magnetically recyclable nanophotocatalysts in photocatalysis-involving processes for organic pollutant removal from wastewater: current status and perspectives. *Environ. Sci. Nano* 11, 1784–1816. doi:10.1039/d3en00906h

Zheng, Z., Min, J., Wang, X., Lung, C. W., Shih, K., and Lo, I. M. C. (2023). Directional separation of highly reductive electrons to the reactive center in a magnetic S-scheme $ZnFe_2O_4$/A-MoS_2 heterojunction for enhanced peroxymonosulfate activation toward pharmaceuticals and personal care product removal. *Environ. Sci. Technol.* 57, 8414–8425. doi:10.1021/acs.est.2c09122

Zhou, A., Liao, L., Wu, X., Yang, K., Li, C., Chen, W., et al. (2020). Fabrication of a Z-scheme nanocomposite photocatalyst for enhanced photocatalytic degradation of ibuprofen under visible light irradiation. *Sep. Purif. Technol.* 250, 117241. doi:10.1016/j.seppur.2020.117241

Zhu, M., Li, J., Chen, M., Li, Y., Zhang, Q., Tang, Y., et al. (2024). Magnetically separable Cd/CdS-$ZnFe_2O_4$/α-Fe_2O_3 Z-scheme heterostructure for boosting the photo-Fenton removal of antibiotic. *J. Alloys Compd.* 988, 174319. doi:10.1016/j.jallcom.2024.174319

Zimmermann, G., Pridoehl, M., Knipping, J., and Roth, P. (2003). Superparamagnetic nanocomposite materials. *Magnetohydrodynamics* 39, 71–76. doi:10.1016/b978-0-323-44923-6.00005-4

Glossary

AOP	Advanced oxidation process
CB	Conduction band
CECs	Contaminant of Emerging Concern
CFD	Computational fluid dynamics
e^-	Electron
Eg	Band gap
h^+	Hole
H_a	Applied magnetic field intensity
HGMSs	High gradient magnetic separators
LISL	Los intensity solar irradiation
Ms	Saturation magnetization
n.s	No specified
OGMSs	Open gradient magnetic separators
Ag	Silver
AgBr	Silver bromide
Ag_2MoO_4	Silver molybdate
A-MoS_2	Ammoniated MoS_2
Ag_3PO_4	Silver phosphate
$Ba_{0.5}Sr_{0.5}TiO_3$	Barium strontium titanate
$BaFe_{12}O_{19}$	Barium ferrite
Bi_2MoO_6	Bismuth molybdate
Bi_2WO_6	Bismuth tungstate
BC	Biochar
Bi_5O_7I	Bismuth pentoxide iodide
$Bi_7O_9I_3$	Bismuth-rich oxyhalide
BiOBr	Bismuth oxybromide
$BiOBr_xI_{1-x}$; $0 \le x \le 1$	Bismuth oxybromo-iodide
$Bi_{24}O_{31}Br_{10}$	Bismuth-rich oxyhalides
BiOCl	Bismuth oxychloride
BiOI	Bismuth oxyiodide
$BiVO_4$	Bismuth vanadate
CdS	Cadmium sulfide
CeO_2	Cerium (IV) oxide
CMCD	Carboxymethyl-β-cyclodextrin
CNT	Carbon nanotube
$CoFe_2O_4$	Cobalt ferrite
Co_3O_4	Cobalt oxide
Cu	Copper
Cu_3ZO	Copper-doped zinc oxide
$CuFe_2O_4$	Copper ferrite
CuO	Copper oxide
d-TiO_2	Defective TiO2
Fe	Iron
Fe_3O_4	Magnetite
FeOOH	Iron oxide hydroxide
FeS_2	Iron disulfide
g-C_3N_4	Graphitic carbon nitride
GO	Graphene oxide
H_2O_2	Hydrogen peroxide
MIL	Materials of Institute Lavoisier
$Mn_{0.6}Zn_{0.4}Fe_2O_4$	Manganese zinc ferrite
$MnFe_2O_4$	Manganese ferrite
SEM	Scanning electron microscope
SL	Solar light
SPM	Superparamagnetic
SSL	Simulated solar light
UV	Ultraviolet
TEM	Transmission electron microscopy
UVA	Ultraviolet-A
UVC	Ultraviolet-C
VB	Valence band
Vis	Visible light
Vp	Particle volume
w/o	Without
μ0	Permeability of free space
MnO_2	Manganese dioxide
MoS_2	Molybdenum disulfide
N-CXTi	carbon xerogel/titanium dioxide
MOF	Metal–organic framework
MWCNT	Multi-walled carbon nanotube
$NiFe_2O_4$	Nickel ferrite
NGAM	Nitrogen-doped graphene aerogel microtube
NiO	Nickel oxide
N-TiO_2	Nitrogen doped titanium dioxide
$^{\bullet}OH$	Hydroxyl radical
P	Phosphorus
PAA	Polyacrylic acid
PANI	Polyaniline
Pd	Palladium
PDS	Peroxydisulfate
PMS	Peroxymonosulfate
PS	Persulfate
Pt	Platinum

SBA15	Type of mesoporous silica
SCF	Spinel cobalt ferrite
SiO_2	Silicon dioxide
$SnFe_2O_4$	Tin ferrite
$SO_4^{\bullet -}$	Sulfate radical
$SrTiO_3$	Strontium titanate
s-Co_3O_4/$NiFe_2O_4$	Starch functionalized s-Co_3O_4/$NiFe_2O_4$
Ti_3C_2	Titanium carbide
TiO_2	Titanium dioxide
TiO_2-P25	Commercial TiO2
TMAC	Titania coated magnetic activated carbon
WO_3	Tungsten trioxide
$Zn_{0.95}Mn_{0.05}S$	Manganese doped zinc sulfide
$ZnFe_2O_4$	Zinc ferrite
ZnO	Zinc oxide
$ZnIn_2S_4$	Zinc indium sulfide
α-Fe_2O_3	Hematite
γ-Fe_2O_3	Maghemite